# NAVAL POSTGRADUATE SCHOOL

## MONTEREY, CALIFORNIA

# THESIS

OCEAN CIRCULATION AND EXCHANGES THROUGH THE
BERING SEA: 1979-2001 MODEL RESULTS

by

Jaclyn L. Clement

June 2005

Thesis Advisor:      Wieslaw Maslowski
Second Reader:       Stephen Okkonen

THIS PAGE INTENTIONALLY LEFT BLANK

| REPORT DOCUMENTATION PAGE | | *Form Approved OMB No. 0704-0188* |
|---|---|---|
| Public reporting burden for this collection of information is estimated to average 1 hour per response, including the time for reviewing instruction, searching existing data sources, gathering and maintaining the data needed, and completing and reviewing the collection of information. Send comments regarding this burden estimate or any other aspect of this collection of information, including suggestions for reducing this burden, to Washington headquarters Services, Directorate for Information Operations and Reports, 1215 Jefferson Davis Highway, Suite 1204, Arlington, VA 22202-4302, and to the Office of Management and Budget, Paperwork Reduction Project (0704-0188) Washington DC 20503. | | |
| **1. AGENCY USE ONLY** *(Leave blank)* | **2. REPORT DATE** June 2005 | **3. REPORT TYPE AND DATES COVERED** Master's Thesis |
| **4. TITLE AND SUBTITLE:** Ocean Circulation and Exchanges Through the Bering Sea: 1979-2001 Model Results | | **5. FUNDING NUMBERS** |
| **6. AUTHOR(S)** Jaclyn L. Clement | | |
| **7. PERFORMING ORGANIZATION NAME(S) AND ADDRESS(ES)** Naval Postgraduate School Monterey, CA 93943-5000 | | **8. PERFORMING ORGANIZATION REPORT NUMBER** |
| **9. SPONSORING /MONITORING AGENCY NAME(S) AND ADDRESS(ES)** N/A | | **10. SPONSORING/MONITORING AGENCY REPORT NUMBER** |
| **11. SUPPLEMENTARY NOTES** The views expressed in this thesis are those of the author and do not reflect the official policy or position of the Department of Defense or the U.S. Government. | | |
| **12a. DISTRIBUTION / AVAILABILITY STATEMENT** Approved for public release; distribution unlimited | | **12b. DISTRIBUTION CODE** A |

**13. ABSTRACT (maximum 200 words)**

A model has been developed and run with sufficiently high resolution (~9 km and 45 levels) and a large enough spatial domain to allow for realistic representation of flow through the narrow and shallow straits in the Bering Sea region. This is potentially important for quantification of long-term mean and time-dependent ocean circulation, and water mass and property exchanges between the Pacific and Arctic oceans. The mean modeled circulation in the Bering Sea is found to be in good agreement with the limited observational data. The Bering Sea Basin, Bering Slope Current, and straits on the northern shelf are identified as highly energetic regions based on eddy kinetic energy fields. Some high biological productivity regions of the northern Bering Sea identified in observational studies are coincident with regions of persistently high energy (up to 2600 $cm^2$ $s^{-2}$ at mid-depth) throughout the annual cycle. Over a twenty-three year interval (1979-2001), mean transport through Bering Strait is estimated to be 0.65 Sv. Comparison of model results with published observations indicates that ocean circulation is not only variable at seasonal to interdecadal scales, but it is also responsive to short-term atmospheric forcing. Comparison with observations of near-bottom salinity indicates that the model is reasonably representing the major water mass properties. The long-term model results for the Bering Sea provide important insights into the ocean circulation and fluxes and they are a useful frame of reference for limited observations that are short-term and/or cover only a small geographic region.

| **14. SUBJECT TERMS** Oceanography, Modeling, Bering Sea | | | **15. NUMBER OF PAGES** 115 |
|---|---|---|---|
| | | | **16. PRICE CODE** |
| **17. SECURITY CLASSIFICATION OF REPORT** Unclassified | **18. SECURITY CLASSIFICATION OF THIS PAGE** Unclassified | **19. SECURITY CLASSIFICATION OF ABSTRACT** Unclassified | **20. LIMITATION OF ABSTRACT** UL |

THIS PAGE INTENTIONALLY LEFT BLANK

**OCEAN CIRCULATION AND EXCHANGES THROUGH THE BERING SEA:
1979-2001 MODEL RESULTS**

Jaclyn L. Clement
Department of Defense Civilian
B.S., University of Tennessee, 2000


Submitted in partial fulfillment of the
requirements for the degree of


**MASTER OF SCIENCE IN PHYSICAL OCEANOGRAPHY**


from the


**NAVAL POSTGRADUATE SCHOOL
June 2005**


Author:          Jaclyn L. Clement


Approved by:     Wieslaw Maslowski
                 Thesis Advisor


                 Stephen Okkonen
                 Second Reader/Co-Advisor


                 Mary L. Batteen
                 Chairman, Department of Oceanography

THIS PAGE INTENTIONALLY LEFT BLANK

# ABSTRACT

A model has been developed and run with sufficiently high resolution (~9 km and 45 levels) and a large enough spatial domain to allow for realistic representation of flow through the narrow and shallow straits in the Bering Sea region. This is potentially important for quantification of long-term mean and time-dependent ocean circulation, and water mass and property exchanges between the Pacific and Arctic oceans. The mean modeled circulation in the Bering Sea is found to be in good agreement with the limited observational data. The Bering Sea Basin, Bering Slope Current, and straits on the northern shelf are identified as highly energetic regions based on eddy kinetic energy fields. Some high biological productivity regions of the northern Bering Sea identified in observational studies are coincident with regions of persistently high energy (up to 2600 $cm^2$ $s^{-2}$ at mid-depth) throughout the annual cycle. Over a twenty-three year interval (1979-2001), mean transport through Bering Strait is estimated to be 0.65 Sv. Comparison of model results with published observations indicates that ocean circulation is not only variable at seasonal to interdecadal scales, but it is also responsive to short-term atmospheric forcing. Comparison with observations of near-bottom salinity indicates that the model reasonably represents the major water mass properties. The long-term model results for the Bering Sea provide important insights into the ocean circulation and fluxes and they are a useful

frame of reference for limited observations that are short-term and/or cover only a small geographic region.

# TABLE OF CONTENTS

THIS PAGE INTENTIONALLY LEFT BLANK

# LIST OF FIGURES

# LIST OF TABLES

THIS PAGE INTENTIONALLY LEFT BLANK

# ACKNOWLEDGMENTS

THIS PAGE INTENTIONALLY LEFT BLANK

# I.  INTRODUCTION

## A.    BACKGROUND OF RESEARCH IN THE BERING SEA

The Bering Sea is characterized by a wide, shallow shelf in the northeast and a deep basin in the southwest. The Aleutian Island Arc forms the southern boundary and Bering Strait, at the northernmost extent, provides the only Pacific connection to the Arctic Ocean.  The Aleutian Island region is strongly influenced by the westward flowing Alaskan Stream, which brings a freshwater river runoff signal from the Gulf of Alaskan (Stabeno et al. 2005).  The strongest connection from the Alaskan Stream to the Bering Sea occurs through Amukta and Amchitka passes and Near Strait.  The deep (to ~4000 m) Bering Sea Basin is bordered to the north by the Bering Slope Current, which flows along the shelf break over a depth of 200-500 m.

The harsh and inaccessible environment has led to limited observational data collection in the Bering Sea. In addition, the circulation scheme has historically been based on intermittent mooring observations at point locations (e.g. Schumacher et al., 1983) and 2-dimensional, low resolution models (e.g. Overland & Roach, 1987; Spaulding et al., 1987).  The relatively shallow (< 55 m) and narrow (~85 km wide) Bering Strait complex is fed by Anadyr and Shpanberg straits to the south.  The ability to quantify the volume and freshwater inputs from Bering Strait northward into the Arctic Ocean is of high importance because these inputs play a significant role in maintaining the Arctic Ocean halocline (Aagaard & Carmack, 1989).  This indicates that the western Arctic sea ice has

a dependence on the Bering Strait water, which provides a cold, fresh surface layer that shields the ice pack from the deeper, warmer Atlantic Layer.  In addition, the Bering Strait water is the primary nutrient source of the Chukchi and Beaufort seas to the north (L. Codispoti, pers. comm.; J. Walsh, pers. comm.).  Calculation of flow through Bering Strait presents several challenges for both observational and modeling studies.  The political boundary between the U.S. and Russia divides the strait and restricts access to potential investigators.  Ice floes with deep drafts are a threat to moorings placed in the upper 40 m of the strait (Roach et al., 1995).  Due to substantial horizontal shear, extrapolation of velocity measurements from one point to total transport is of uncertain validity, although the use of multiple current meters and regression techniques increases confidence in transport estimates (Aagaard et al., 1985).  While political boundaries and ice draft do not significantly impede modeling efforts, the geomorphology (i.e. width and depth) of the strait and a large ocean to the north and south are challenging as they require a combination of high resolution and large domain to realistically represent flow.

Currently, many global ocean circulation models either have a closed Bering Strait or instead use some type of prescribed conditions.  Goosse et al. (1997) found that their treatment of a closed versus open Bering Strait had a significant impact on model results. Specifically, with an open Bering Strait, modeled oceanic and sea ice transports through Fram Strait increased to more realistic values.  Also the sea ice edge in the Bering Sea was more realistically positioned further north due to warmer water

advection across the Bering Sea. In addition, the modeled freshwater budgets of the Greenland and Norwegian seas and of the Atlantic Ocean were enhanced by the Bering Strait throughflow. Although general circulation models (GCMs) may not have high enough resolution to explicitly represent the exchanges through Bering Strait, results presented here indicate that GCMs can benefit from high-resolution regional modeling that can realistically account for flow through narrow straits. Improved understanding of ocean circulation and sea ice conditions in data-limited regions should facilitate more realistic simulations in GCMs. This goal was central to the study, but in addition, it was expected that results in the Bering Strait region would provide insight into the mean state and variability of water mass and property fluxes, such as heat and freshwater, into the Arctic Ocean. Upstream (southward) from Bering Strait, field observations have shown an east-west increase in salinity and nutrient concentrations (Walsh et al., 1989; Grebmeier & Cooper, 1995). Anadyr Water, Bering Shelf Water, and Alaska Coastal Water are three primary water masses flowing over the northern Bering Sea shelf (Walsh et al. 1989). In the west, deeper Pacific Water is generally upwelled onto the shelf within the Gulf of Anadyr, with relatively high salinity and nutrient content (Anadyr Water). A less saline and nutrient-rich, water mass (Bering Shelf Water) is found in the central region of the northern Bering Sea, while a strong gradient defines the warmer (in summer), nutrient-poor Alaska Coastal Water to the east (Coachman, 1987; Grebmeier et al., 1988).

A limited number of modeling studies have concentrated on the northern Bering Sea (e.g. Overland & Roach, 1987; Spaulding et al., 1987; Nihoul et al., 1993). These studies have proven useful in simulating the major circulation features of the region. However, they have been limited by low spatial resolution and small domains with lateral boundary conditions prescribed in close proximity to the region of interest. In addition, these studies were integrated only for a short period of time (1-3 months). Recent advancements in computing capability and updated bathymetry information have allowed the development of a relatively high-resolution (~9 km and 45 levels), large domain model encompassing the Bering Sea, which has been spun-up for 48 years and integrated with realistic forcing for an additional 23 years.

The overarching goal of this research is to quantify the long-term mean and variability of the circulation and water mass properties over short (monthly) to long (decadal) time scales across the data-limited northern Bering Sea and through Bering Strait using this pan-Arctic coupled ice-ocean model. One of the specific objectives in this study was to improve understanding of the flow and transports through Anadyr, Shpanberg, and Bering straits (locations shown on Figure 3). Model results are validated against observational data including salinity and nutrient concentrations in the Bering Sea, in addition to salinity and temperature measurements and volume transport estimates in Bering Strait.

## B. SIGNIFICANCE TO NAVAL OPERATIONS

Recent satellite observations (Cavalieri et al., 1997; Johannessen et al. 1999) and modeling studies show a significant decline in sea ice extent during the last few decades. The sharpest decline has occurred during the past few years. Unpublished results from the model used in the present study reveal declines not only in ice extent and area, but also ice thickness and volume. It is anticipated that decreasing sea ice will allow for more ship traffic in the Arctic Ocean and surrounding seas. Regions which were previously accessible only by sub-surface and ice breaking vessels may become open to various surface ships. Changing sea ice conditions will also affect the acoustic properties of the Arctic, which is important for anti-submarine warfare operations. In addition, commercial shipping vessels may begin to take advantage of ice-free conditions in certain areas to reduce transit time.

These implications make it necessary to investigate the complex and relatively under-studied arctic and sub-arctic environment. It is important for defense strategists to be prepared for a rapid shift from generally temperate operations to an increase in polar operations in the Arctic.

THIS PAGE INTENTIONALLY LEFT BLANK

## II. MODEL DESCRIPTION

The coupled sea ice-ocean model has a horizontal grid spacing of 1/12° (or ~9 km) and 45 vertical depth layers with 8 levels in the upper 50 m. The high vertical resolution, especially in the upper water column, allows for more realistic representation of the shallow Arctic and sub-Arctic shelves as compared to previous models, which were only 2-dimensional (e.g. Overland & Roach, 1987; Spaulding et al., 1987). In addition, the high-resolution horizontal grid permits calculation of flow through the narrow straits of the northern Bering Sea. The model domain (Fig. 1) contains the sub-Arctic North Pacific (including the Sea of Japan and the Sea of Okhotsk) and North Atlantic oceans, the Arctic Ocean, the Canadian Arctic Archipelago (CAA) and the Nordic Seas. The region of interest, the Bering Sea, is therefore, far away from the artificially closed lateral boundaries in the North Pacific at $30^{\circ}$N, greatly reducing potential boundary effects. Model bathymetry is derived from two sources: ETOPO5 at 5 km resolution for the region south of $64^{\circ}$N and International Bathymetric Chart of the Arctic Ocean (IBCAO; Jakobsson et al., 2000) at 2.5 km resolution for the region north of $64^{\circ}$N. The ocean model was initialized with climatological, 3-dimensional temperature and salinity fields (PHC; Steele et al., 2000) and integrated for 48 years in a spinup mode. During the initial spinup, daily-averaged annual climatological atmospheric forcing derived from 1979-1993 reanalysis from the European Centre for Medium-Range Weather Forecasts (ECMWF) was used for 27 years. Then an additional run was performed using repeated

7

1979 ECMWF annual cycle for 6 years and then 1979-1981 interannual fields for the last 15 years of spinup. This approach is especially important to establishing realistic ocean circulation representative of the time period at the beginning of the actual interannual integration. This final run with realistic daily-averaged ECMWF interannual forcing starts in 1979 and continues through 2001. Results from this integration (23-years) are used for the analyses in this paper. Yukon (and other Arctic) river runoff is included in the model as a virtual freshwater flux at the river mouth. However, in the Gulf of Alaska the freshwater flux from runoff (Royer, 1981) is introduced by restoring the surface ocean level (0-5 m) to climatological (PHC) monthly mean salinity values over a monthly time scale (as a correction term to the explicitly calculated fluxes between the ocean and overlying atmosphere or sea ice). Additional details on the model including sea ice, river runoff, and restoring have been provided elsewhere (Maslowski et al., 2004).
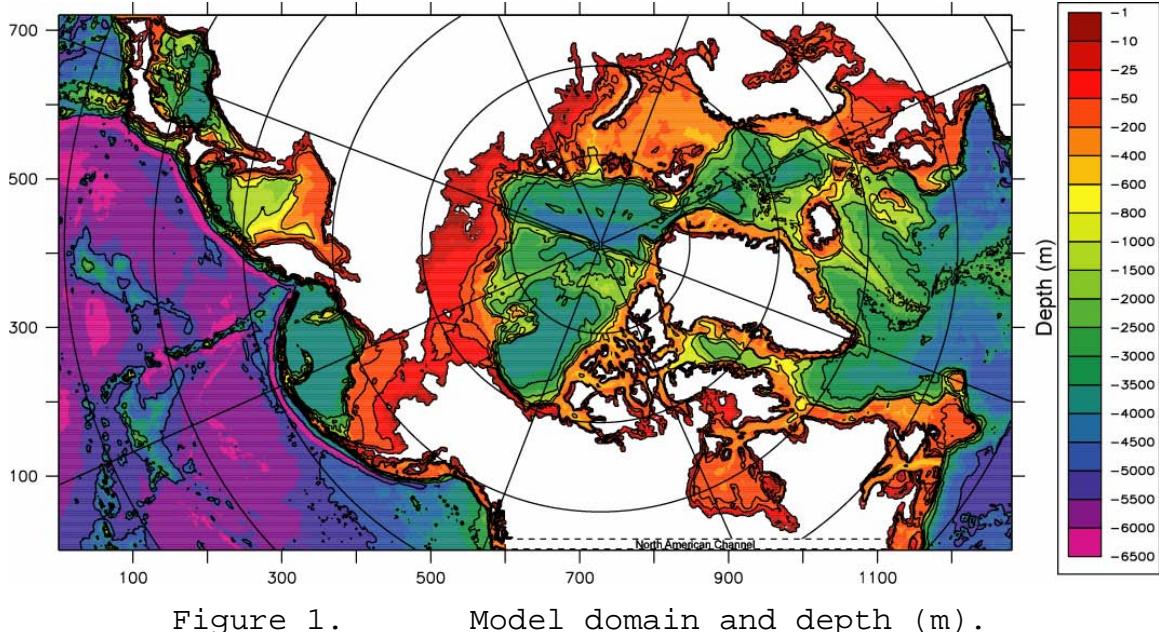


Figure 1.        Model domain and depth (m).

# III. RESULTS

## A.    THE BERING SEA GENERAL CIRCULATION

The Bering Sea is bordered to the south by the Aleutian Island Arc and the associated westward-flowing Alaskan Stream (Fig. 2).  The Alaskan Stream is the strongest current in the region and has a twenty-three-year (1979–2001) mean modeled transport of 45–56 Sv, increasing as it moves west.  Throughflow from the Alaskan Stream into the Bering Sea primarily occurs through Amchitka and Amukta passes and Near Strait (locations shown in Fig. 3).  The Bering Sea Basin has a generally cyclonic circulation, with the Bering Slope Current flowing northwestward along and above the continental northern slope.  On the northern Bering Sea shelf, the circulation is generally northward and intensification occurs in narrow straits such as Bering, Anadyr, and Shpanberg, as well as along the western boundary (Anadyr Current).
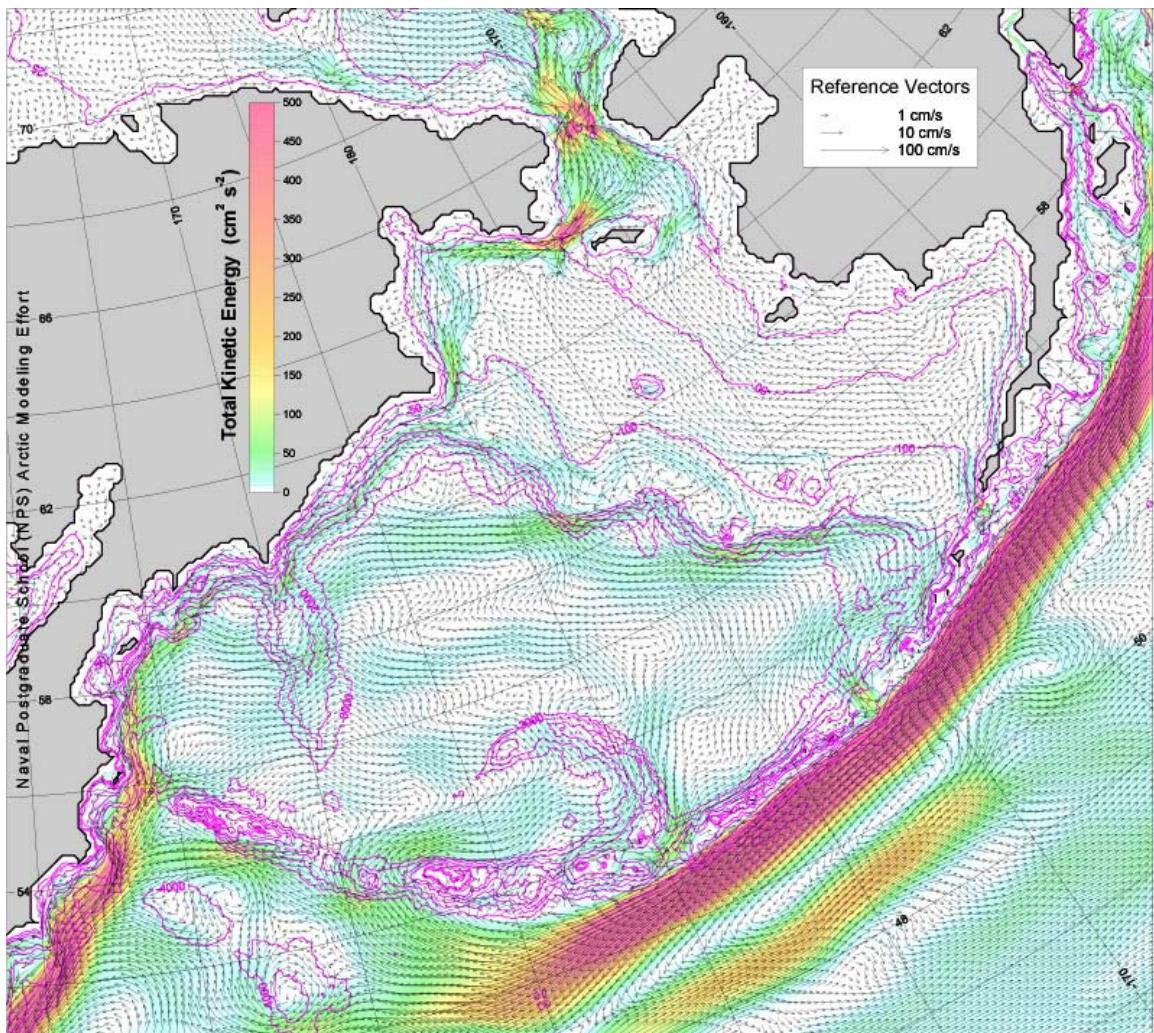
Figure 2. Twenty-three-year (1979–2001) mean circulation and total kinetic energy in the upper 65 m of the water column. Twenty-five percent of vectors are shown. Color shading represents the total kinetic energy (cm$^2$ s$^{-2}$) calculated as 0.5*(u$^2$+v$^2$).
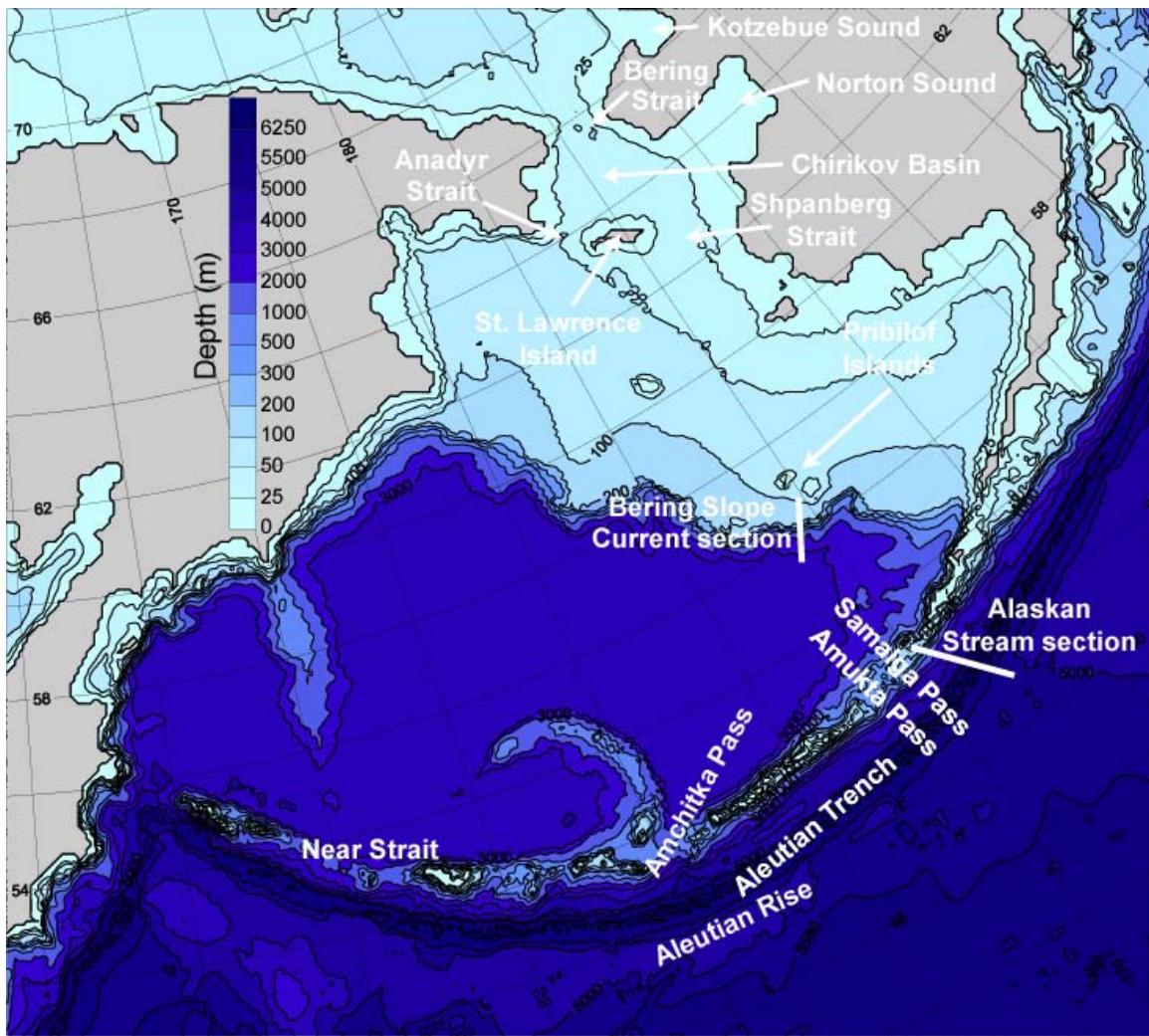
Figure 3.      Model bathymetry, locations of various topographic features, and locations of model cross-sections.

## 1.   Alaskan Stream and Aleutian Island Arc

The Alaskan Stream is the narrow (~50-80 km wide), deep western boundary current of the eastern portion of the sub-arctic gyre.   The twenty-three-year mean velocity in the upper 50 m reaches over 80 cm s$^{-1}$ in a cross-section just east of Samalga Pass at ~168$^{o}$W (Fig. 4).    Mean velocities in the upper 1000 m are $\geq$ 10 cm s$^{-1}$, which indicates that deep flow contributes significantly to the

11

overall total volume transport of the current. The mean temperature in the upper 50 m is 6-8.5 $^{\circ}$C, decreasing to ~3 $^{\circ}$C at a depth of 1000 m (Fig. 4). The Alaskan Stream carries a low salinity signal (S = 31.8-32.2) from the Gulf of Alaska in the upper 100 m.

The Alaskan Stream modeled volume transport increases as the current moves westward. At 164$^{\circ}$W the total transport is 45 Sv, while at 174$^{\circ}$W the transport is 56 Sv due to northward entrainment of the eastward flowing Sub-arctic Current. The eastward flowing Sub-arctic Current lies just south of the Alaskan Stream (Fig. 2). The topography of the Aleutian Rise steers a portion of this current northward where it meets and strengthens the Alaskan Stream.
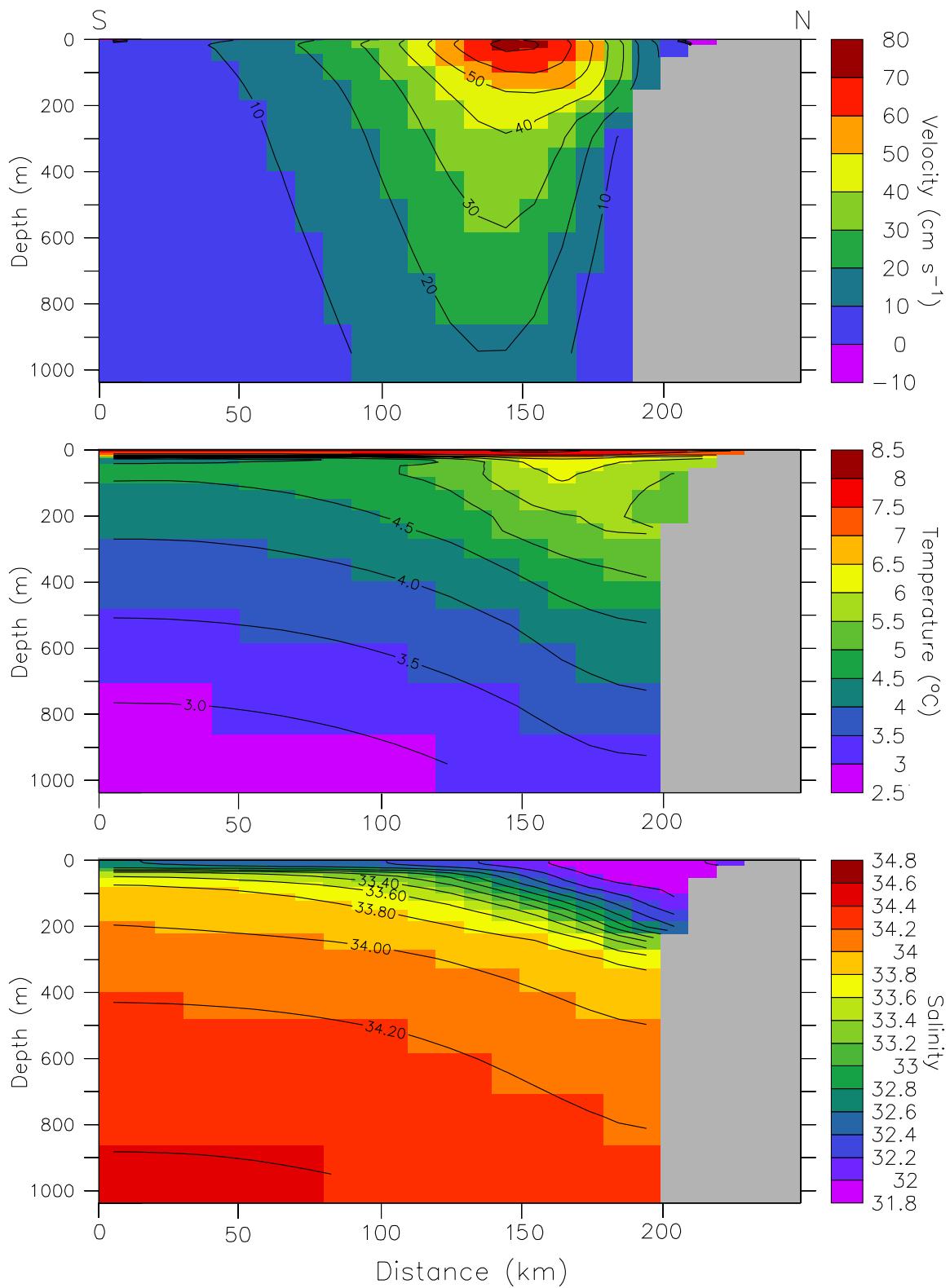
Figure 4.    Alaskan Stream cross-section of twenty-
three-year (1979-2001) mean velocity, temperature,
and salinity.

Flow through the relatively shallow central Aleutian passes is important for determining the oceanographic dynamics of the southeastern Bering Sea (Overland et al., 1994; Stabeno and Reed, 1994).  In addition, much of the freshwater (S < 32) is thought to exit the Alaskan Stream before it reaches the western passes (Stabeno et al., 2005).  Twenty-three-year mean modeled volume transport through Amukta Pass is 1.6 Sv with a standard deviation of 0.8 Sv (location shown in Fig. 3).  This is lower than the estimate given by Stabeno et al. (2005) of ~4 Sv based on 4 moorings placed in the pass from May 2001 to September 2003.  The difference in mass transport may be related to differences between the model bathymetry and the actual bathymetry.  In addition, the horizontal resolution of the model (~9 km) is likely limiting the proper representation of the flow through this narrow pass (~90 km wide). Finally, strong tidal currents occur in this region (Stabeno et al., 2005) and at present the model does not include tides.

## 2.   Bering Sea Circulation

The circulation in the Bering Sea Basin has been described as spatially complex and temporally variable (Reed, 1995).  In the mean state, the circulation is generally cyclonic with intensification along the Russian coast (Kamchatka Current) and within the Bering Slope Current (Fig. 2).  The main inflow into the basin is through Near Strait and to a lesser extent through Amchitka and Amukta passes.  The Kamchatka Current carries most of the outflow southward along the Kamchatka Peninsula.

The Bering Slope Current, flowing northwestward along the northern edge of the basin, has a twenty-three-year mean (1979-2001) modeled transport of ~3.0 Sv along a cross-section just south of the Pribilof Islands. The mean velocity core (speeds up to 11 cm $s^{-1}$) is located in the upper 200 m over the shelf break (Fig. 5). There is a distinct front located along the 200 m isobath, which divides the colder and fresher shelf water from the warmer, saltier basin water. The halocline and a subsurface temperature maximum exist between 200-300 m.
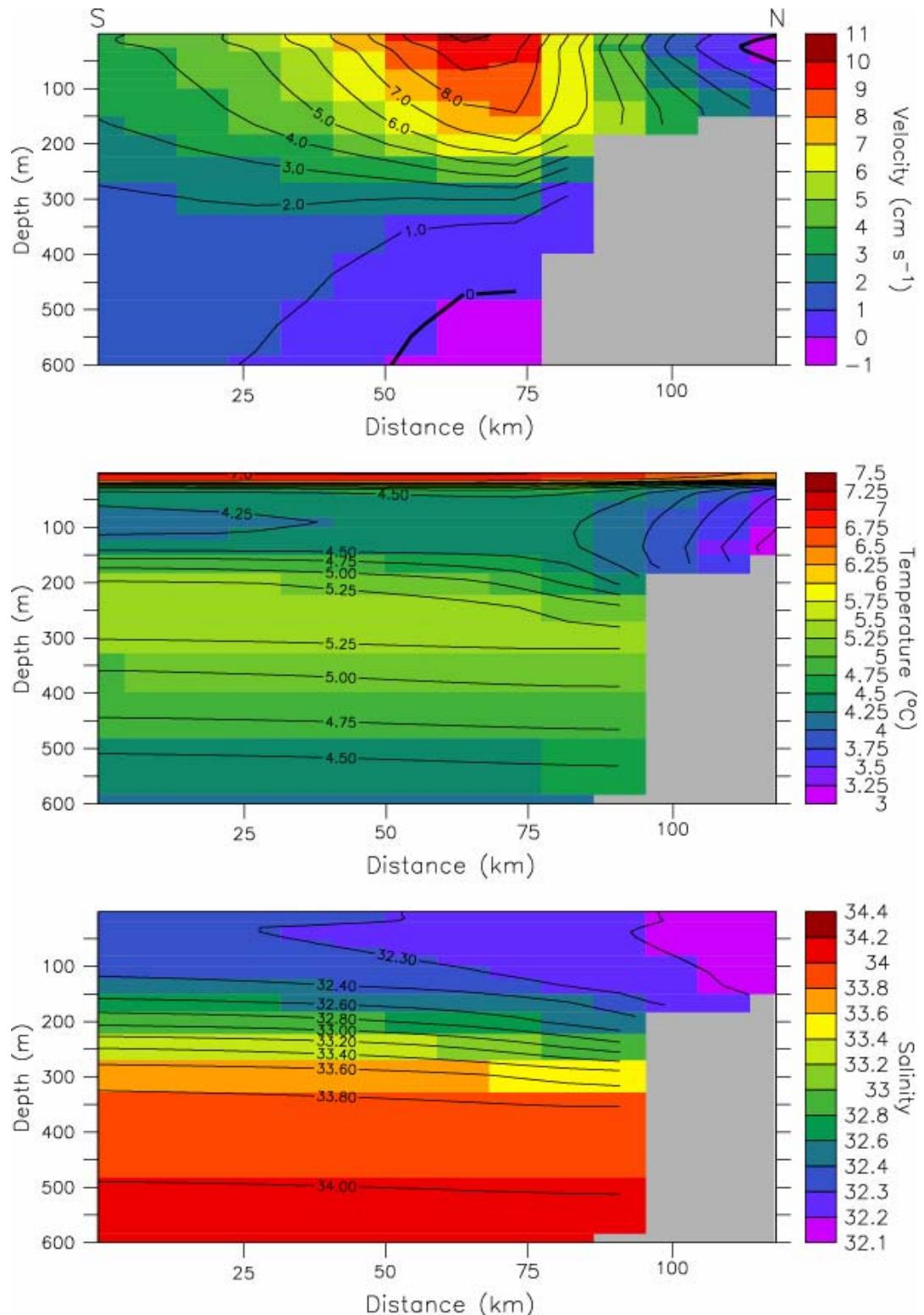
Figure 5.        Bering Slope Current cross-section of
twenty-three-year (1979-2001) mean velocity,
temperature, and salinity.  The section is located
just south of the Pribilof Islands.

The 23-yr (1979-2001) modeled mean circulation in the upper 65 m on the northern Bering Sea shelf (Fig. 2) is generally in agreement with previous studies such as Schumacher et al. (1983). In their study a current meter mooring (64$^{\circ}$N, 171.9$^{\circ}$W) showed strong Anadyr Strait flow (~0.156 m s$^{-1}$) directed northeastward toward the Chirikov Basin during November 1980 through June 1981. At another mooring located 40 km south of St. Lawrence Island (63$^{\circ}$N, 171$^{\circ}$W) flow was eastward at ~0.036 m s$^{-1}$, while only ~0.005 m s$^{-1}$ was recorded 60 km to the southwest of the island (63.1$^{\circ}$N, 173.1$^{\circ}$W). As in the Schumacher et al. (1983) dataset, the model (Fig. 2), shows high northeastward velocity in Anadyr Strait, lower velocity directed eastward south of St. Lawrence Island and sluggish flow to the southwest of the island (note the color shading in Fig. 2). There is close agreement between model and data on these key features, although the model output also shows stronger flow along isobaths (e.g. along the 50-m isobath and between the 60- and 70-m isobaths) across the central and eastern shelf south of St. Lawrence Island. Unfortunately, very little published observational data are available to confirm these modeled features. The model represents the circulation in the Chirikov Basin (north of St. Lawrence Island) as a sweeping flow bathymetrically steered toward Bering Strait, instead of a coastal jet moving straight to the western edge of Bering Strait, as depicted in Hermann et al. (2002). While it is possible that there is a narrow coastal jet, which may not be fully resolved using a 9-km grid cell, it seems likely that cold and saline Anadyr Water moving through Anadyr Strait (as represented in Figs.

17

24 and 25) would follow the local bathymetry into the deeper central portion of the Chirikov Basin.

Circulation varies seasonally (model output not shown) with higher velocities during spring and summer in the northern Bering Sea (NBS; defined as north of 62°N, south of 67°N and between 165°W and 175°W). Model output shows lower velocities during winter as a result of sea ice cover, although, the middle shelf (south of the NBS and less than 500 m deep) actually intensifies during autumn and winter, possibly in relation to ice edge dynamics. It is also worth noting that just south of St. Lawrence Island eastward flow becomes more organized and stronger during spring and summer (not shown), which is not as apparent in the 23-year mean.

## 3.   Bering Sea Eddy Kinetic Energy in 1987

With a horizontal grid cell spacing of approximately 9 km, this model is able to resolve eddies with diameters as small as 36 km. As such, the eddy kinetic energy (EKE = $(u'^2 + v'^2)/2$) distribution in the Bering Sea was calculated from daily fluctuations (u', v'), referred to the annual mean. EKE is an important model parameter which, in the physical world, commonly represents regions of active mixing and associated increased biological productivity. Realistic representation of EKE in a model is often challenging, but when achieved can provide useful information about the dynamics and productivity in a region. Observational estimates of EKE on the Bering shelf are not readily available, hence the following discussion

serves to establish a quantitative, yet possibly incomplete, reference.

The mean velocity components for the 23-year time series, $\bar{u}$ and $\bar{v}$, were calculated and then subtracted from the daily velocity values to obtain u' and v'. The year 1987 was chosen because it was characterized by an average transport through Bering Strait and it does not appear strongly biased toward any particular climate regime in the North Pacific or Arctic Ocean. At the surface (0 - 5 m), annual mean EKE is highest (up to 2700 $cm^2$ $s^{-2}$) along the Alaskan Stream, in the Bering Sea Basin, and in Bering and Anadyr straits (Fig. 6). Lesser, but still significant EKE of approximately 60 $cm^2$ $s^{-2}$, is found across the middle shelf. Below the wind-driven, surface layer at 20-26 m, there is much reduced EKE across the middle shelf with some weak intensification along isobaths (Fig. 7). However, EKE remains very high along the Alaskan Stream and in the northern Bering Sea, especially in Bering and Anadyr straits. Several large eddy-like features with diameters of 100-200 km can be seen in the Bering Sea Basin.
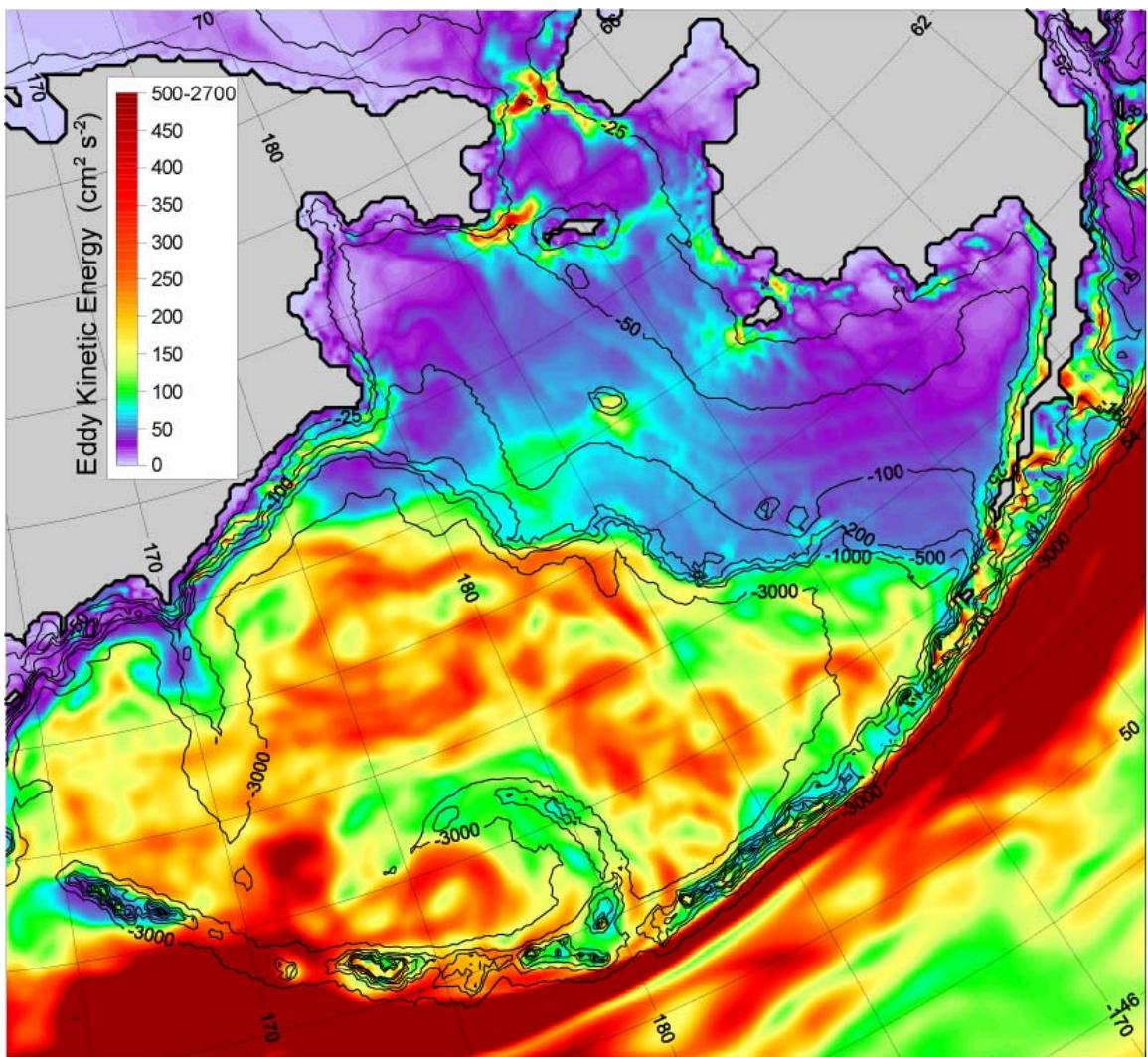
Figure 6.　　　Annually-averaged eddy kinetic energy (cm$^2$ s$^{-2}$) calculated from daily 1987 snapshots (against 23-year mean) at the surface level (0-5 m)
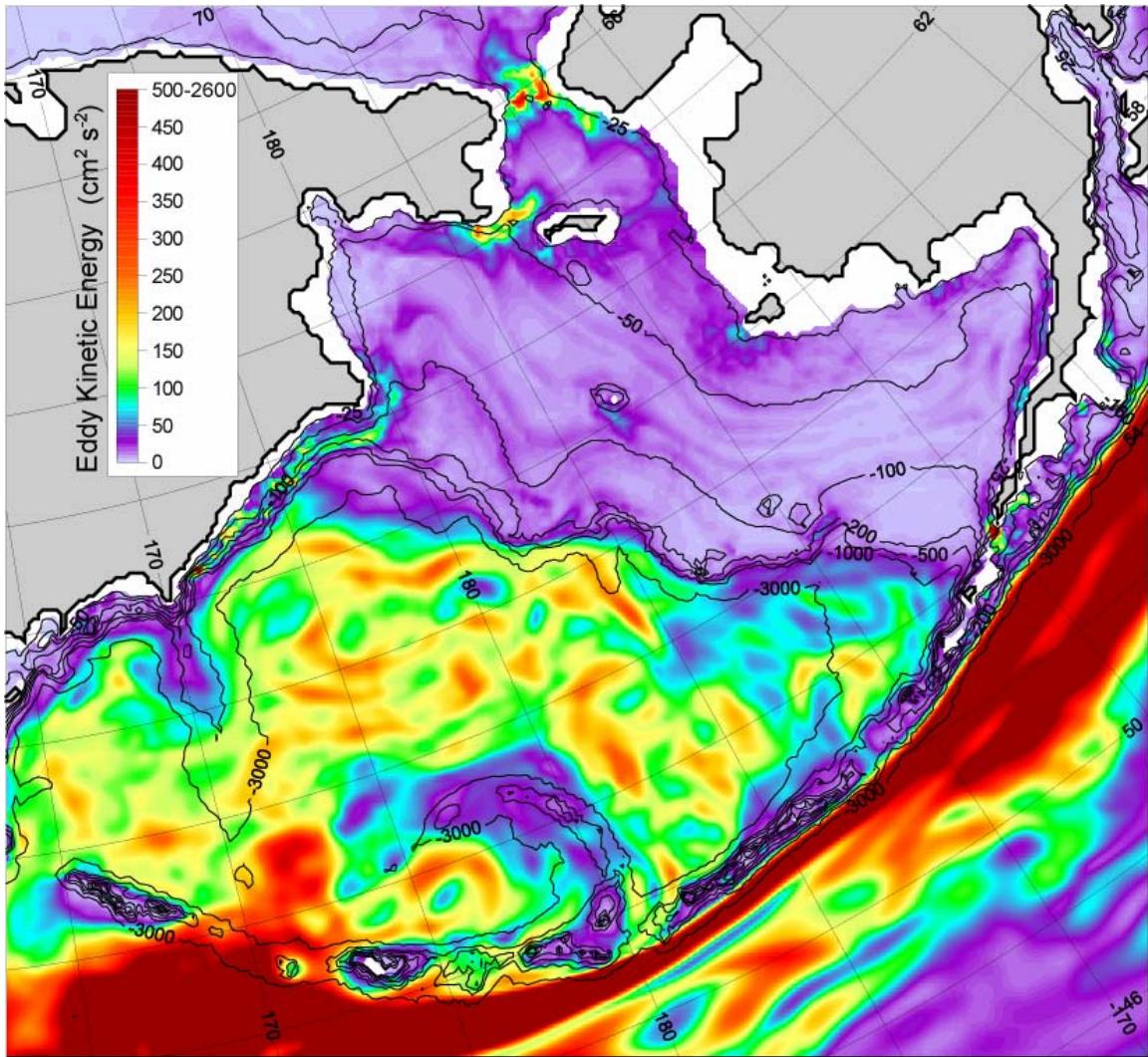
Figure 7.          Annually-averaged eddy kinetic energy ($cm^2$ $s^{-2}$) calculated from daily 1987 snapshots (against 23-year mean) at 20-26 m

## B.    FOCUS ON THE NORTHERN BERING SEA AND BERING STRAIT

The northern Bering Sea is characterized by a wide, shallow shelf with multiple narrow straits.  The schematic mean circulation of the region, along with the bathymetry is shown in Figure 8.  Flow is generally northward across the shelf toward the Arctic Ocean.  Water moving northward must either pass through Anadyr Strait to the west of St.

Lawrence Island or the shallower Shpanberg Strait to the east before reaching Bering Strait.
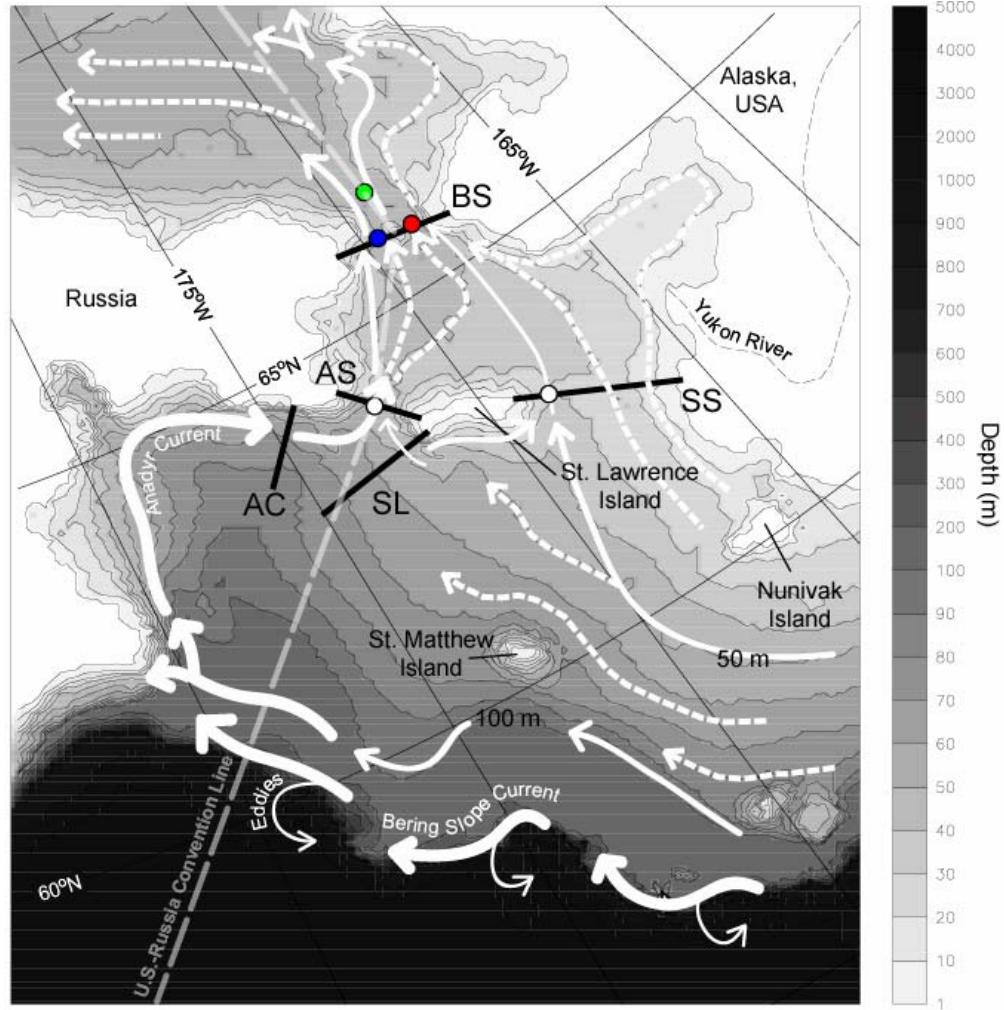


Figure 8.      Schematic of mean circulation in the Bering Sea after Coachman (1993), Stabeno et al. (2001), and Hermann et al. (2002).  Dashed arrows are proposed based on the results of this study.  Thick black lines indicate model cross-sections: BS (Bering Strait), AS (Anadyr Strait), SS (Shpanberg Strait), AC (Anadyr Current), and SL (St. Lawrence Island).  Mooring locations are shown as colored circles (Western Channel, blue; Eastern Channel, red; and North Central, green).  White circles indicate model stations in the deepest part of Anadyr Strait and Shpanberg Strait.  There are also model stations in the same locations as the moorings in the Western and Eastern Channels of Bering Strait.

### 1.    Interannual Circulation Variability


Interannual variation in the Bering Sea circulation is examined by comparing the year of highest modeled volume transport through Bering Strait (1979) with the year of lowest modeled transport (1994).  The mean velocity in the upper 50 m of the region shown in Fig. 9 during 1979 is 0.044 m s$^{-1}$, while in 1994 it is only 0.033 m s$^{-1}$ (Fig. 10). A notable difference is much less organized flow in the east and the weaker flow in the central Bering Sea during 1994 compared to 1979.  The difference in vector fields for 1979-1994 (Fig. 11) also indicates significantly weaker flow during 1994 in the northern and eastern regions, as well as along the Bering Slope Current (BSC).  Differences along the BSC are likely due to variations in eddy activity.  Across the region the mean difference between the two years is 0.025 m s$^{-1}$ or ~70% of the 23-yr mean. These differences in flow are attributed to differences in wind speed and direction.  Annually averaged wind fields (not shown) for 1979 and 1994 show much stronger wind (2 – 3 m s$^{-1}$) out of the north in the vicinity of Bering Strait during the year of lowest transport (1994).  The stronger northerly winds appear to impede northward oceanic transport through the strait and upstream.  A different situation occurs in 1979 with weaker winds (1.5 – 2 m s$^{-1}$) out of the northeast, which have less of an influence on northward transport.
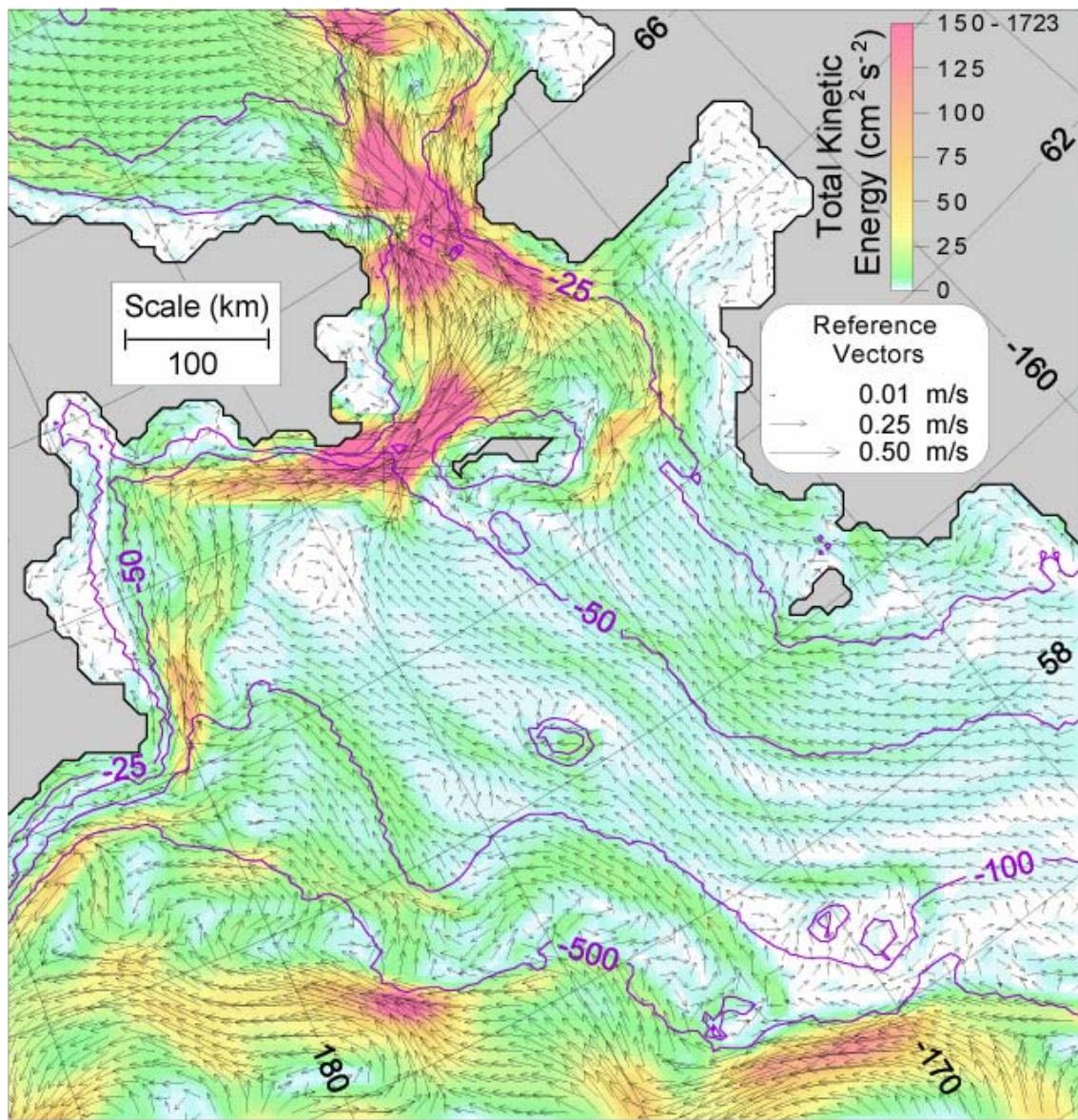
Figure 9.    Mean annual velocity in the upper 50 m during the year of highest (1979) northward transport through Bering Strait over the 23-year model integration (1979-2001).  Twenty-five percent of vectors are shown. Color shading represents the total kinetic energy ($cm^2 s^{-2}$) calculated as $0.5*(u^2+v^2)$.
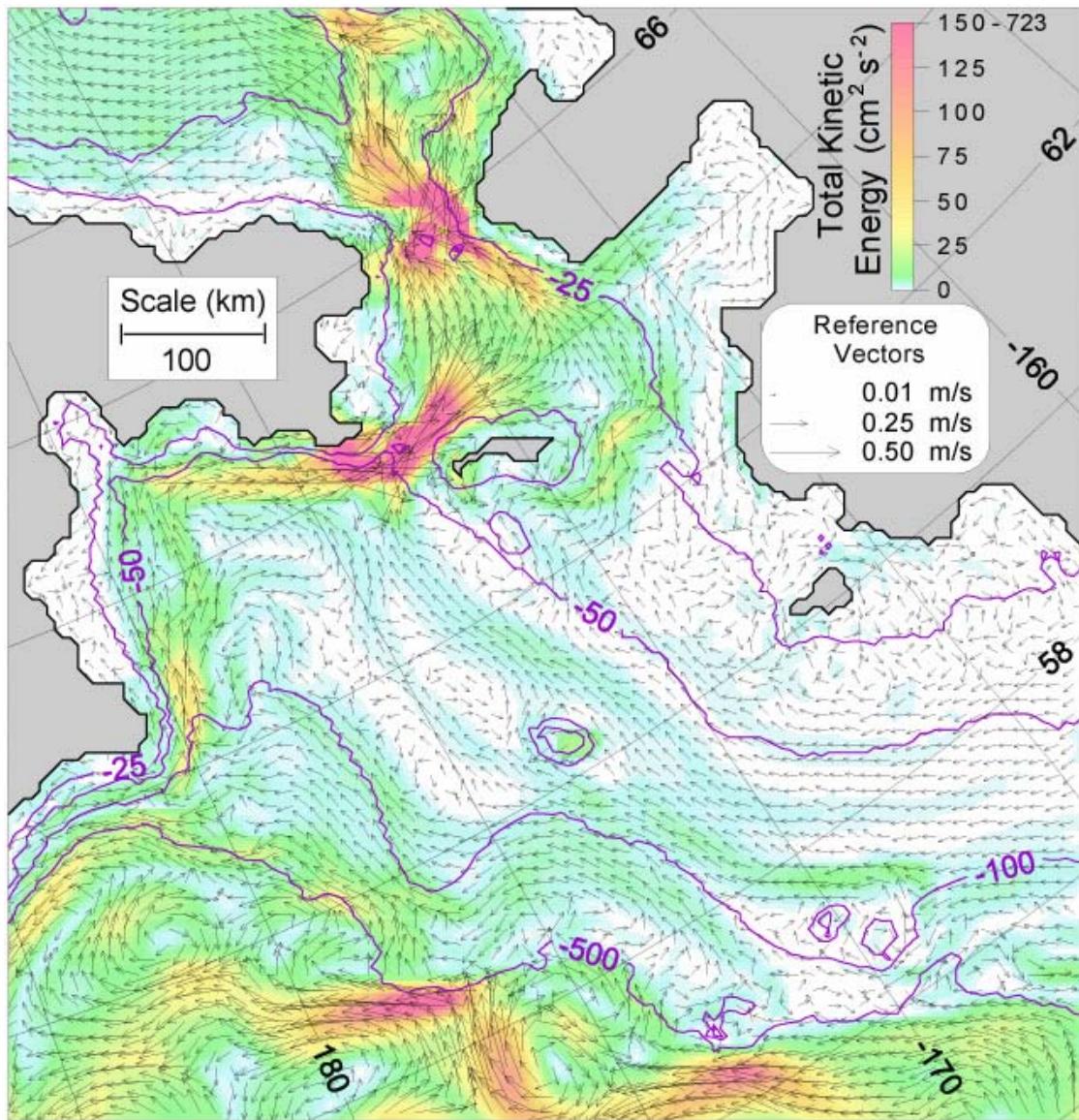
Figure 10.      Mean annual velocity in the upper 50 m
during the year of lowest (1994) northward transport
through Bering Strait over the 23-year model
integration (1979-2001).  Twenty-five percent of
vectors are shown. Color shading represents the
total kinetic energy ($cm^2 s^{-2}$) calculated as
$0.5*(u^2+v^2)$
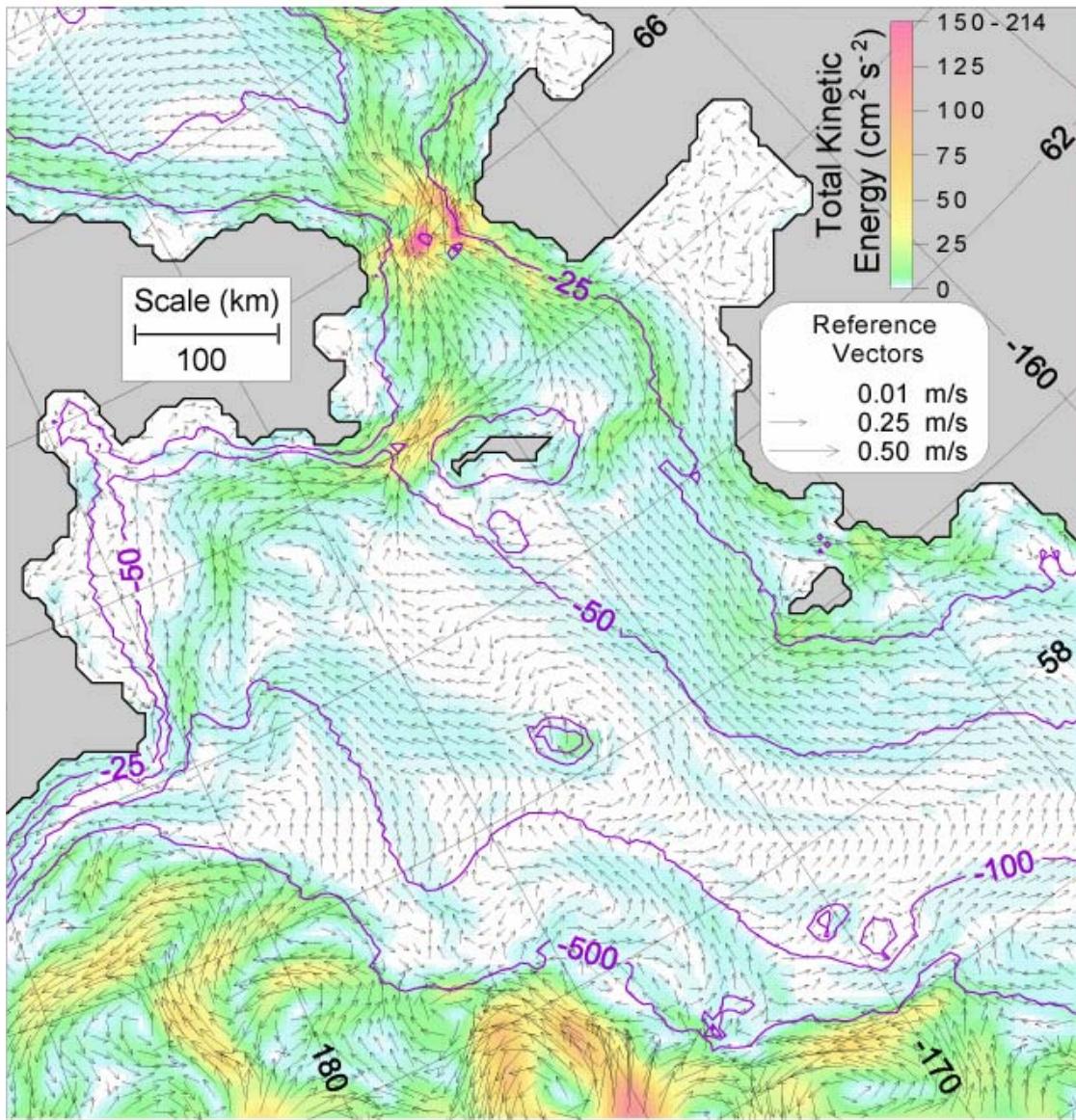
Figure 11.     Difference in the annual velocity during 1979 minus 1994 in the upper 50 m.  Twenty-five percent of vectors are shown. Color shading represents the total kinetic energy ($cm^2 s^{-2}$) calculated as $0.5*(u^2+v^2)$

2.   **Seasonal Eddy Kinetic Energy Variability and Regional Differences during 1987**

Seasonal changes in EKE in the surface layer are visible across the Bering shelf with highest values in

26

autumn and winter (Figs. 12 and 13).  Bering and Anadyr straits maintain relatively high EKE throughout the year, but peak during autumn.  The area directly south of St. Lawrence Island is also a region of increased EKE, while north of the island in the Chirikov Basin a distinct decrease is observed.  Below the surface at 20-26 m depth, there is a sharp decrease in EKE across the middle shelf (Fig. 13), similar to the annual mean.  Again, the EKE in the northern straits and along the Bering Slope Current remains elevated.
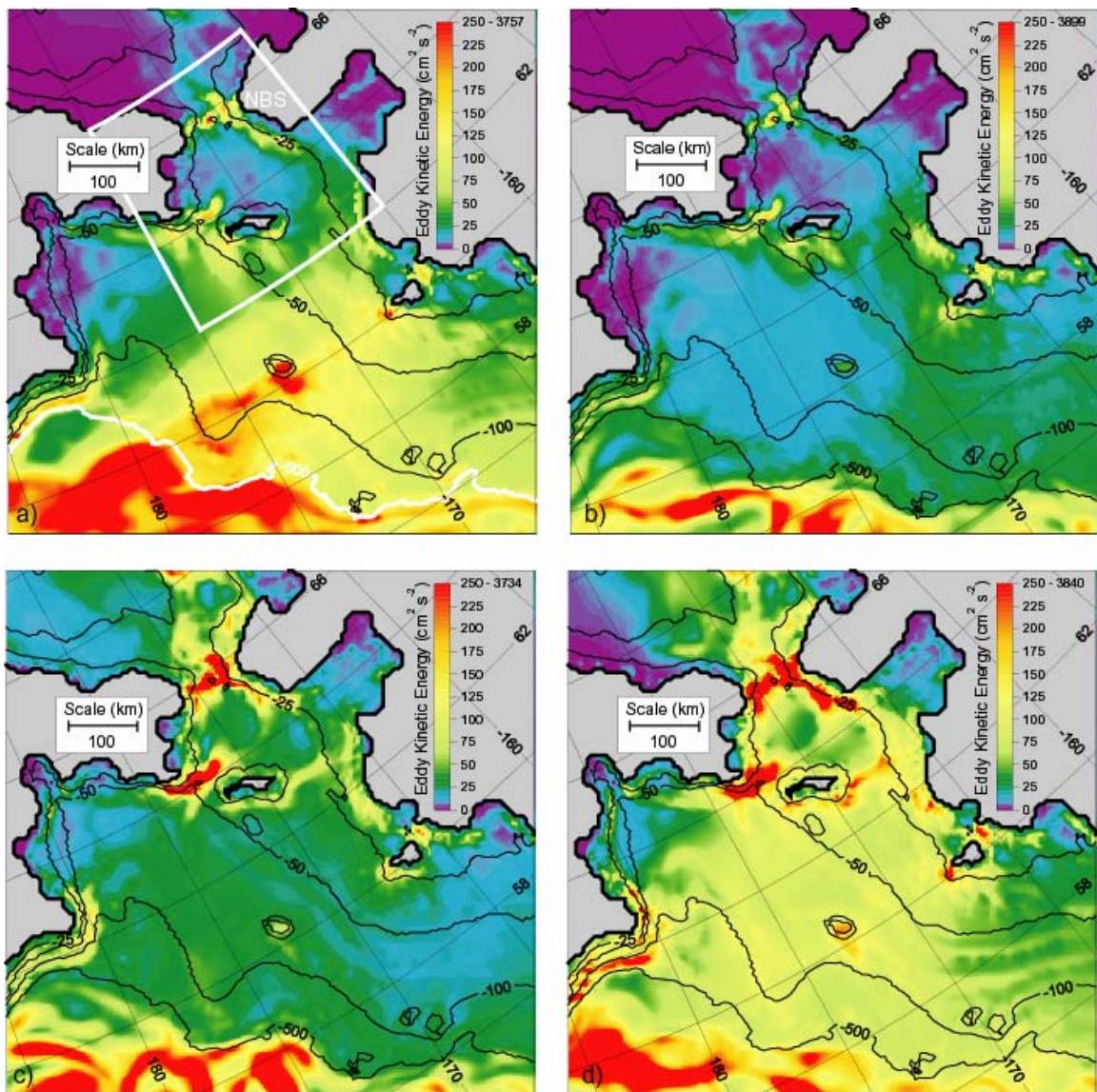
Figure 12.      Seasonally-averaged EKE at the surface calculated from daily 1987 snapshots (against 23-year mean):  (a) Winter (J-F-M) average, (b) Spring (A-M-J) average, (c) Summer (J-A-S) average, (d) Autumn (O-N-D) average.
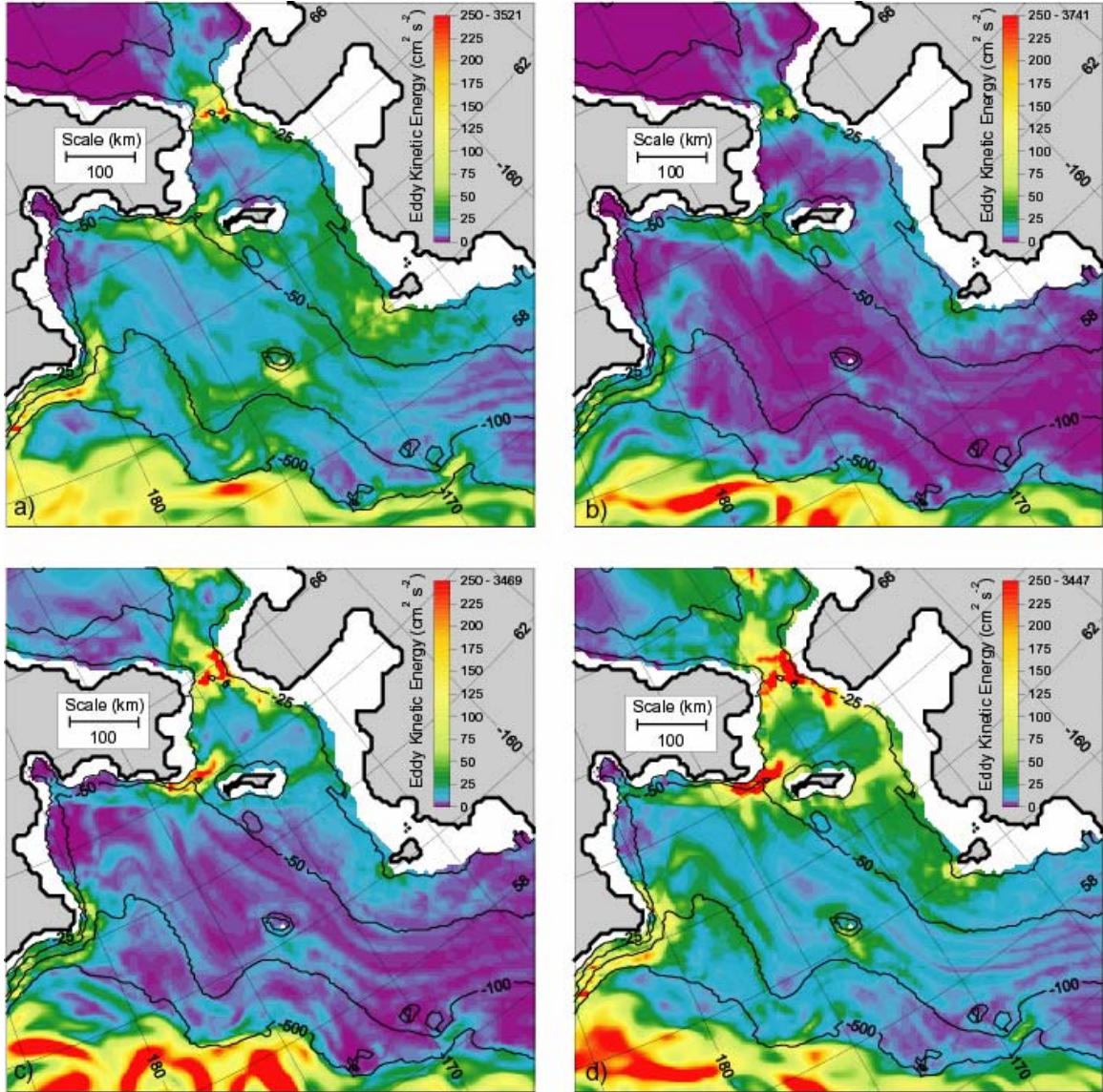
Figure 13.        Seasonally-averaged EKE at 20-26 m (level 5)
        calculated from daily 1987 snapshots (against 23yr
        mean):  (a) Winter (J-F-M) average, (b) Spring (A-M-
        J) average, (c) Summer (J-A-S) average, (d) Autumn
        (O-N-D) average.

        Upon noting the differences in EKE for various regions
of the Bering Sea, daily area-averaged EKE for the northern
Bering Sea, the middle shelf, and the entire region
(respectively, red, blue, and black lines in Fig. 14) were
computed.  The northern Bering Sea (NBS) region, defined in
Fig. 12a, shows relatively low surface EKE in the first

part of 1987 (red line), while the middle shelf region (south or the NBS and north of the 500-m isobath) has high EKE (blue line), likely due to passing storms and ice edge location (Fig. 14a). Spring EKE is low for all regions followed by a strong increase in the NBS during summer. Finally, the autumn season shows the highest values for the NBS with peaks lasting approximately 5-10 days, a synoptic period similar to the duration of Bering Sea cyclonic systems. Similar peaks show up for the middle shelf and the entire region, but they are only about two-thirds the magnitude of that observed in the NBS. Below the surface at 20-26 m, the highest EKE for most of the year, except for the NBS in autumn, is over the entire region (Fig. 14b). This is likely due to the strong influence of eddies of the Bering Slope Current (BSC) propagating along the slope and into the basin. The middle shelf is much lower in energy throughout most of the year. Using a regional model of the southeastern Bering Sea, Hermann et al. (2002), also found frequent eddy activity along the BSC and much less on the southeastern part of the shelf. The shallow shelf waters of the NBS continue to have the highest energy during autumn with deeper water (20-26 m) peaks that are approximately half those at the surface.
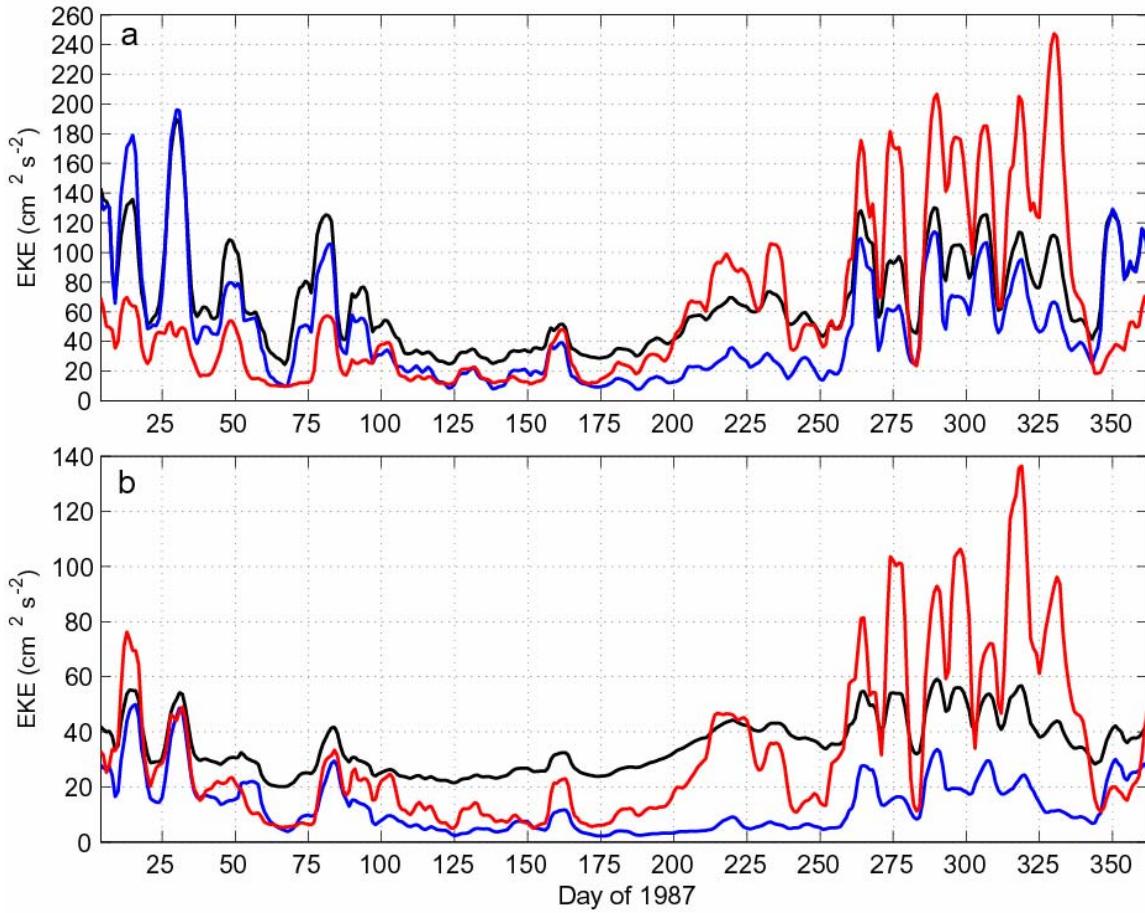
Figure 14.      Daily variability of Bering Sea (area-averaged) EKE during 1987 (against 23yr mean): (a) surface level, (b) 20-26 m (level 5).  Data is presented with 7-day smoothing.  Entire region (black), Northern Bering Sea (NBS; red), mid-Bering shelf (south of the NBS region with depth less than 500m; blue).  See Figure 12a for region boundaries.

## 3.    Volume, Freshwater, and Heat Transports

Five vertical cross-sections shown in Figure 8 are analyzed for volume, freshwater, and heat transport in this section of text and compared to the limited observational data that are available.  Based on data collected during 1990-1994, Roach et al. (1995) estimate the mean northward volume transport through Bering Strait to be 0.83 Sv

(maximum error of 30% or ±0.25 Sv, 1 Sv = $10^6$ $m^3$ $s^{-1}$). The modeled mean northward transport during the same time is 0.58 Sv with a standard deviation of ±0.21 Sv, which is in the lower range of the observational estimate. The mean of the entire integration (1979-2001) is 0.65 Sv with a standard deviation of ±0.23 Sv (Table 1). Bering Strait (BS) and Anadyr Strait (AS) have similar annual cycles, showing higher monthly mean transport in summer up to ~0.95 and 0.80 Sv, respectively (Fig. 15). This is consistent with measurements made by Roach et al. (1995) in Bering Strait, who reported higher velocities in the spring and summer months with winter values about 25% lower. Shpanberg Strait (SS) and Anadyr Current (AC) show relatively less variation over the annual cycle, with slightly higher northward transport in summer (Fig. 15). Transport is generally northward across the St. Lawrence section (SL) except during February and March when the flow is reversed. This may be due to changes in wind forcing and density gradients caused by sea ice formation (Schumacher et al., 1983). Transport across SL is relatively low compared to most other sections and is high in summer and highest in November and December. This second peak in early winter may be due, in part, to winter storms that frequently occur in this region (Overland and Pease, 1982) prior to the southward advancement of sea ice cover, which tends to reduce the impact of wind forcing on the ocean.

| Section | Mean | Max | Min | S.D. |
|---------|------|------|-------|------|
| BS | 0.65 | 1.28 | 0.11 | 0.23 |
| AS | 0.52 | 0.95 | 0.07 | 0.17 |
| SS | 0.13 | 0.73 | -0.20 | 0.13 |
| AC | 0.37 | 0.97 | -0.70 | 0.22 |
| SL | 0.13 | 1.23 | -0.39 | 0.22 |

Table 1.    Statistics based on monthly mean time series
of 23-year mean net volume transport through various
sections shown in Fig. 8.
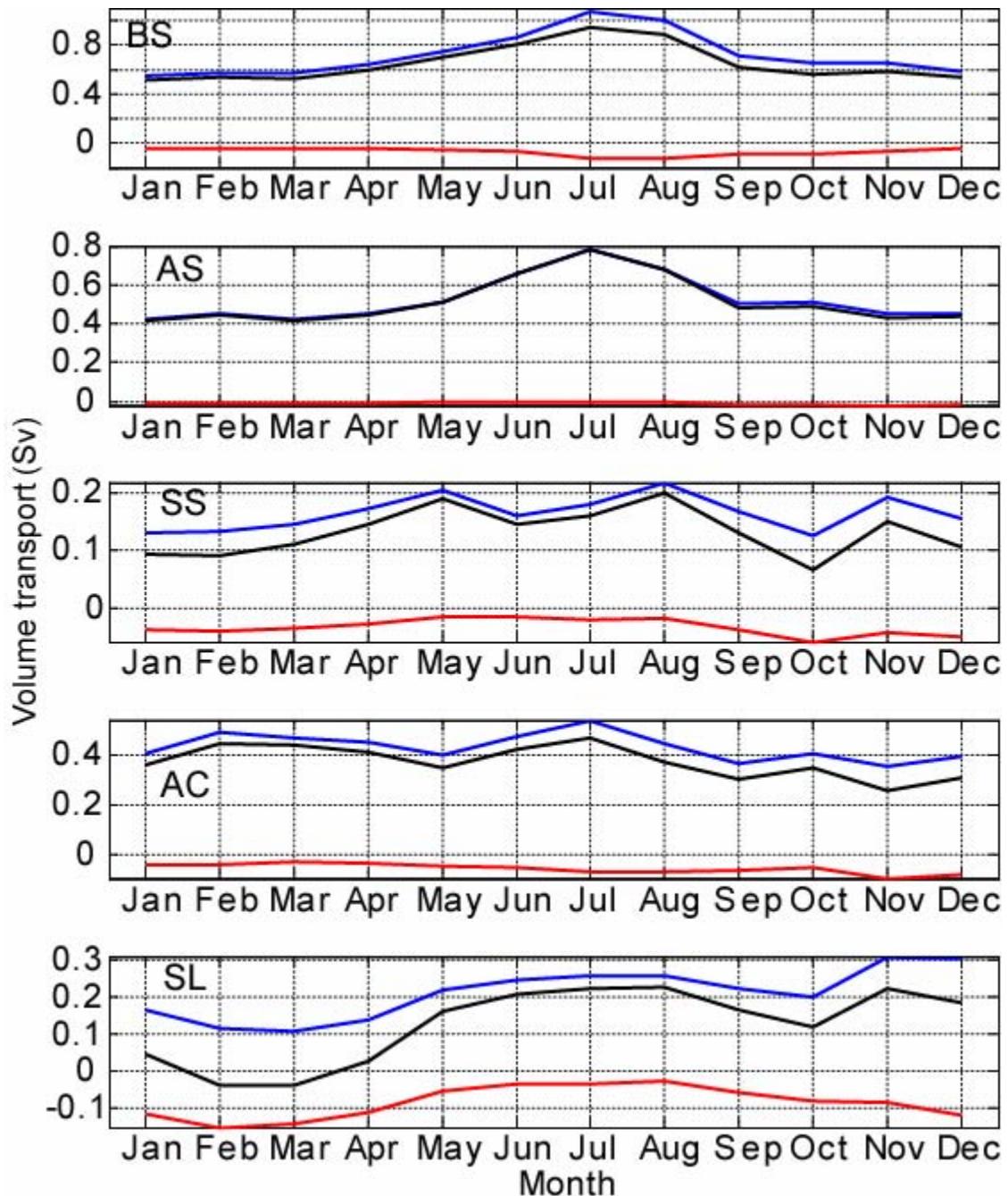
Figure 15.        Annual cycle volume transport through Bering Sea sections (see Figure 8 for section locations). Monthly means are calculated from a 23-year time series (1979-2001). Positive (blue line) fluxes represent flow to the North or East according to the model grid, while negative (red line) fluxes represent flow to the South or West. Black lines represent net flow.

Maximum positive heat transport (referenced to $-0.1^{\circ}C$) occurs in summer and early autumn at all sections (Fig. 16). The net amount of heat transported northward across Shpanberg Strait is ~60% of that across Anadyr Strait even though the volume flux through SS is only 25% of AS (Tables 2 and 3). This is consistent with observations of warmer water in the eastern Bering Sea as compared to the western regions (Coachman, 1987; Grebmeier et al., 1988). In general, the annual cycle of heat transport does not correlate well with volume transport, mainly due to seasonal changes in water temperature.
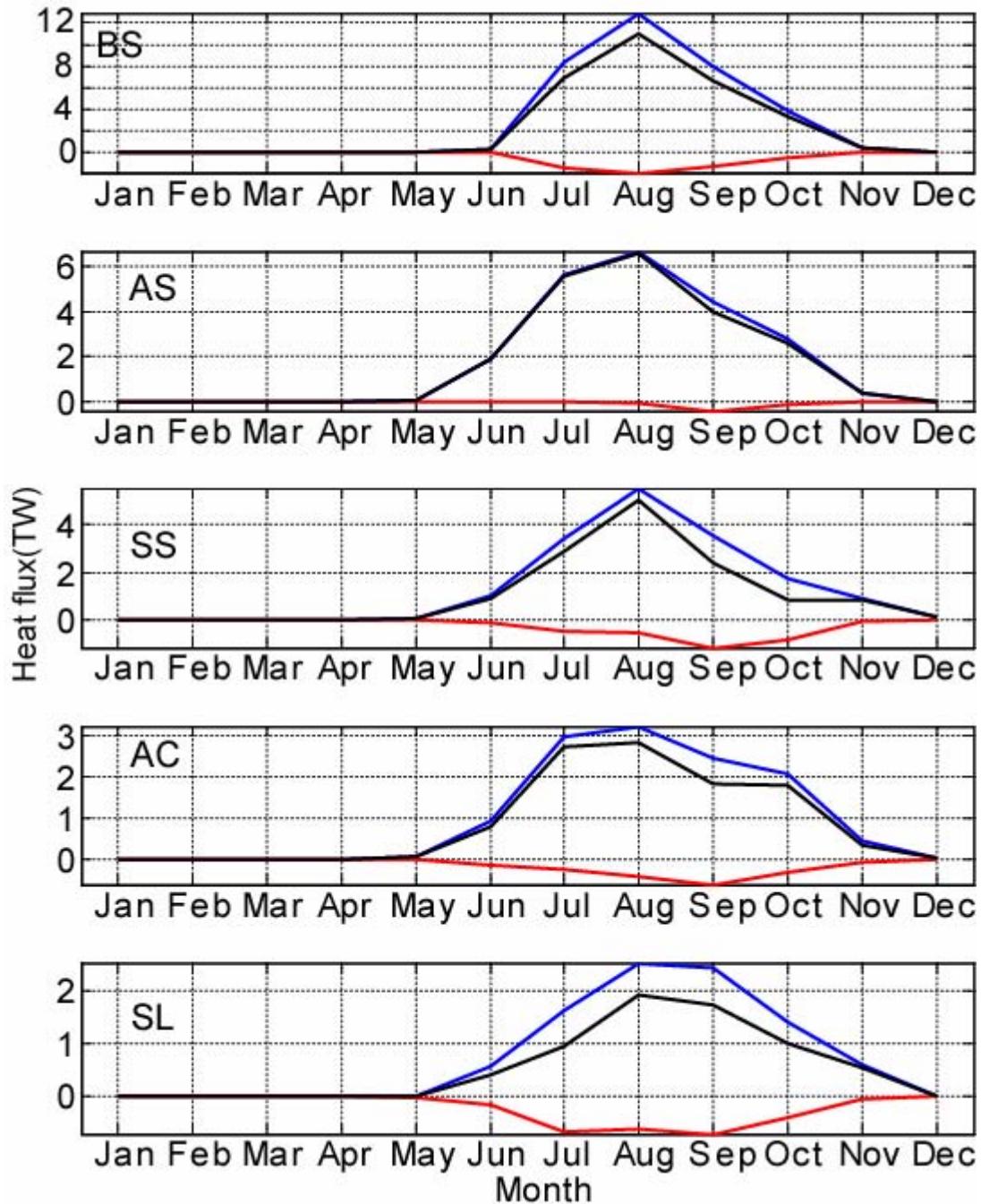
Figure 16.        Annual cycle heat fluxes through Bering Sea
sections (see Figure 8 for section locations).
Monthly means are calculated from a 23-year time
series (1979-2001).  Positive (blue line) fluxes
represent flow to the North or East according to the
model grid, while negative (red line) fluxes
represent flow to the South or West.  Black lines
represent net flow.  The reference temperature is –
0.1(°C).

| Section | Vol Net | Vol In | Vol Out |
|---------|---------|--------|---------|
| BS | 0.65 (0.23) | 0.72 (0.25) | -0.07 (0.03) |
| AS | 0.52 (0.18) | 0.53 (0.17) | -0.01 (0.01) |
| SS | 0.13 (0.13) | 0.17 (0.10) | -0.03 (0.03) |
| AC | 0.37 (0.22) | 0.43 (0.18) | -0.06 (0.07) |
| SL | 0.13 (0.22) | 0.21 (0.16) | -0.09 (0.09) |

Table 2.    Twenty-three-year mean volume transport (Sv) through selected sections.  Calculations are for the entire water column.  Standard deviation is shown in parenthesis in the lower right-hand corner of each cell.

| Section | Heat Net | Heat In | Heat Out |
|---------|----------|---------|----------|
| BS | 2.37 (4.12) | 2.82 (4.78) | -0.45 (0.70) |
| AS | 1.75 (2.52) | 1.81 (2.55) | -0.06 (0.16) |
| SS | 1.09 (2.19) | 1.36 (2.24) | -0.27 (0.55) |
| AC | 0.86 (1.39) | 1.01 (1.48) | -0.15 (0.26) |
| SL | 0.55 (1.06) | 0.76 (1.11) | -0.22 (0.43) |

Table 3.    Twenty-three-year mean heat transport (TW) through selected sections.  Heat is referenced to – $0.1^{\circ}$C.  Calculations are for the entire water column. Standard deviation is shown in parenthesis in the lower right-hand corner of each cell.

Freshwater transport (referenced to a salinity of 34.8) is highest in summer for all sections except SL, where it peaks again in late autumn, similar to the annual cycle of volume transport (Fig. 17).  Freshwater transport across Bering Strait is lowest in winter and early spring (30-40 mSv, $10^{-3}$ Sv) and highest in July (~70 mSv) in the

annual cycle.  The 23-year mean freshwater transport is ~47 mSv with approximately ~37 mSv coming from the upstream Anadyr Strait and ~10 mSv coming from Shpanberg Strait (Table 4).  These relative contributions to the BS freshwater transport are similar to the volume transport contributions.
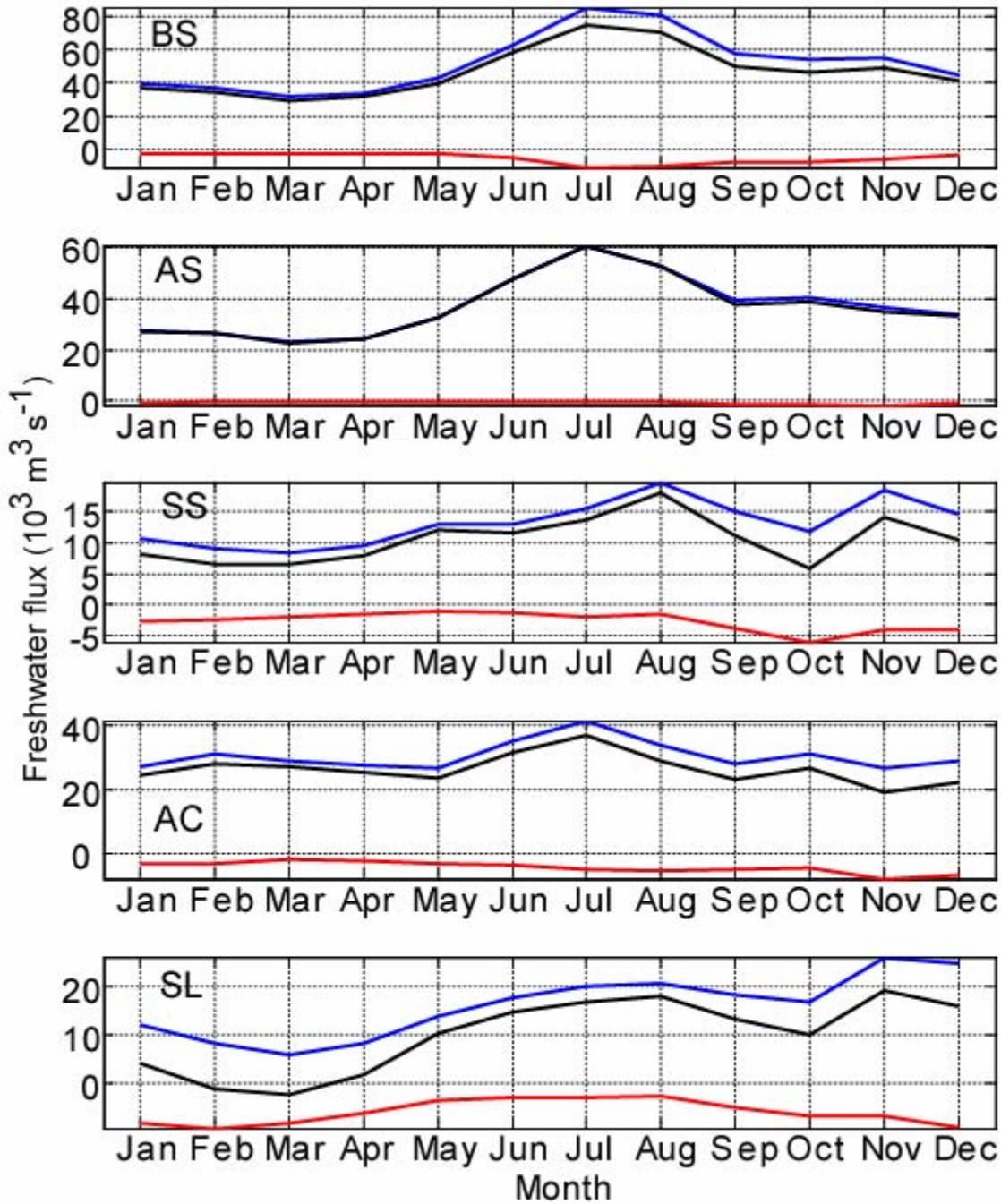
Figure 17.     Annual cycle freshwater fluxes through
     Bering Sea sections (see Figure 8 for section
   locations).  Monthly means are calculated from a 23-
   year time series (1979-2001).  Positive (blue line)
   fluxes represent flow to the North or East according
   to the model grid, while negative (red line) fluxes
    represent flow to the South or West.  Black lines
   represent net flow.  The reference salinity is 34.8.

| Section | FW Net | FW In | FW Out |
|---------|--------|-------|--------|
| BS | 46.84 (20.44) | 52.09 (22.94) | -5.25 (3.21) |
| AS | 36.61 (15.65) | 37.31 (15.35) | -0.70 (0.92) |
| SS | 10.55 (11.82) | 13.29 (10.01) | -2.74 (3.24) |
| AC | 26.27 (16.52) | 30.50 (13.82) | -4.22 (5.76) |
| SL | 9.97 (17.27) | 15.98 (13.41) | -6.01 (6.15) |

Table 4. Twenty-three-year mean freshwater transport ($10^3$ $m^3$ $s^{-1}$) through selected sections. Freshwater is referenced to a salinity of 34.8. Calculations are for the entire water column. Standard deviation is shown in parenthesis in the lower right-hand corner of each cell.

Time series over 23 years for the five vertical sections show seasonal, as well as interannual, variability in flow across the northern Bering shelf (Fig. 18). The net 23-year mean annual volume transport across Bering Strait is 0.65 Sv, with 0.72 Sv moving northward and a slight but annually regular component (0.07 Sv) moving southward (Table 2 and Fig. 18). The minimum of the interannual signal (0.48 Sv) was reached in 1994 and the interannual maximum (0.78 Sv) in 1979, indicating interannual variability of approximately +0.15 Sv. A similar estimate of +0.2 Sv was made by Coachman et al. (1993) based on observational studies during the ISHTAR program. Monthly mean transports (black line in Fig. 18) are often greater than 1 Sv with a low of 0.11 Sv in December 1997 and a high of 1.28 Sv in August 1999. Examination of instantaneous transports across Bering Strait (calculated every model time step of 480 seconds)

40

reveals even stronger wind-driven variability, from 2.7 Sv northward to 2.5 Sv southward (data not shown).
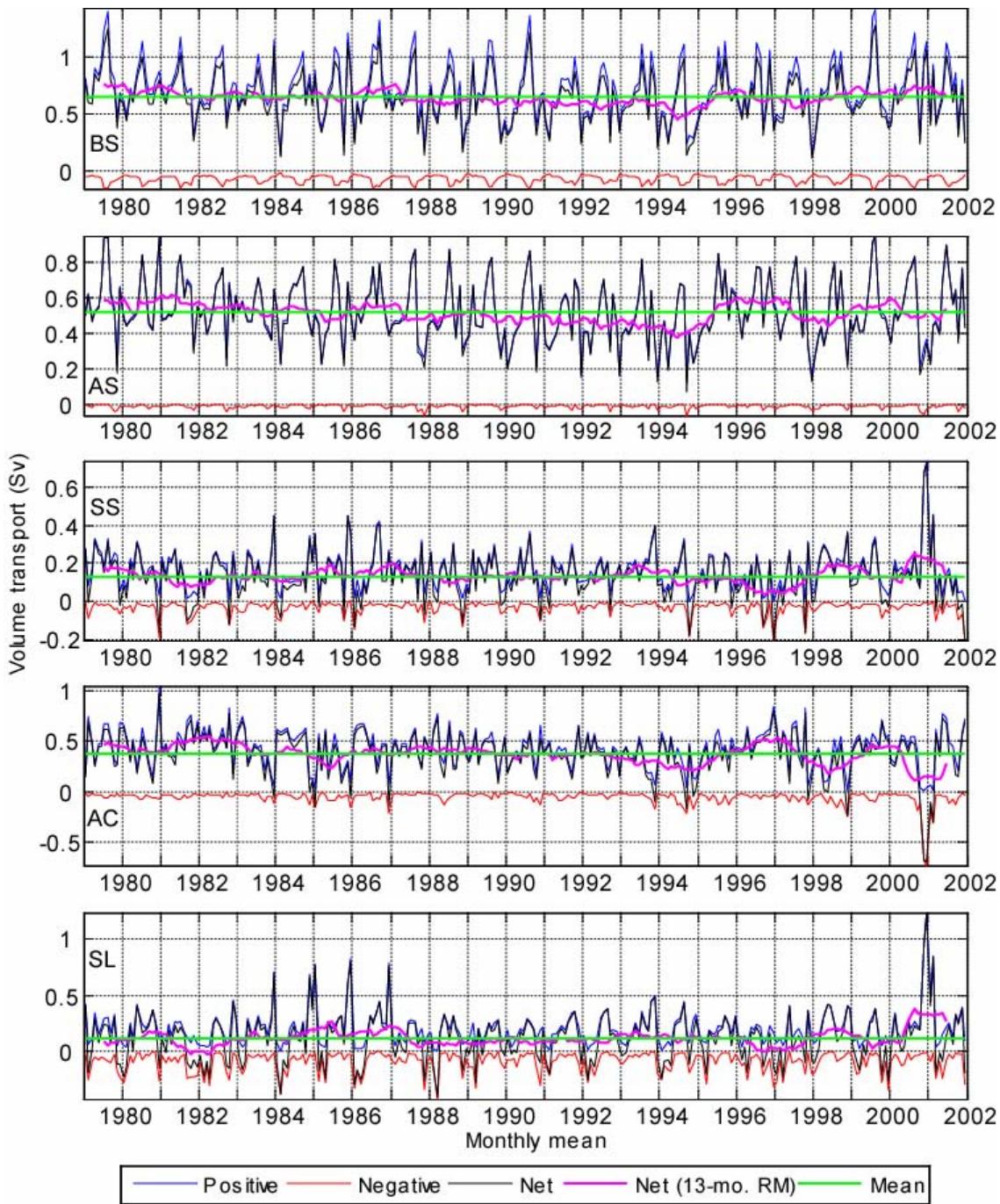
Figure 18.         Monthly mean volume transport over a 23-year
        time series (1979-2001).   Positive (blue line)
    fluxes represent flow to the North or East according
        to the model grid (see Figure 8), while negative
        (red line) fluxes represent flow to the South or
    West.   Black lines represent net flow.   The smoothed
    net flux (thick magenta line) is a 13-month running
    mean.   The 23-yr mean is represented by the green
                            line.

Transports across SS, AC, and SL all exhibited flow reversals (Fig. 18). The most notable flow reversal (up to -0.70 Sv) in the 23-year time series occurred across the AC section during November and December 2000. Flow continued to be westerly across the northwestern Bering Sea until March 2001. This episode was also evident in the AS, SS, and SL sections, with greatly increased northwestward flow across the northern Bering shelf. This event also coincided with observations of reduced sea ice conditions during winter of 2000-01 (Fig. 19). Satellite observations during February 1999 and 2001 show that ice concentrations were very low during 2001 as compared to a more typical year, 1999 (Fig. 19ab; Clement et al., 2004). The model shows a similar ice distribution in the two years, except for slightly lower ice concentrations (80-95%) instead of solid > 95% ice cover detected during Feb. 1999 (Fig. 19cd). These areas of slightly reduced ice cover concentrations in the model might be representative of the realistic presence of leads and relatively warm ocean currents. The strong flow reversal, which peaked in November and December 2000 (see Figure 18), and northwestward movement of sea ice occurred relatively quickly over the course of a few months during winter 2000-01. The cause of this event is most likely wind forcing, as shown in Figure 20. While previous studies indicate that prevailing winds are northerly or northeasterly in the northern Bering Sea during winter (Muench and Ahlnäs, 1976; Pease, 1980; Overland, 1981), a very different scenario took place during winter 2000-01. Figure 20 depicts the ECMWF wind forcing field (used in the model) averaged over

the 2-month peak in flow reversal (November and December
2000) as compared to the more typical year (November and
December 1998).   In 1998, wind was out of the north with
speeds of 3 - 4 m s$^{-1}$ in the vicinity of Bering Strait and
up to 4.5 m s$^{-1}$ south of St. Lawrence Island.  In contrast,
during 2000 much stronger wind speeds of 5 - 6.5 m s$^{-1}$
occurred near Bering Strait, with speeds up to 9.3 m s$^{-1}$ in
the Gulf of Anadyr.   The average magnitude difference
between 1998 and 2000 winter winds was 3.0 m s$^{-1}$ and the
wind direction was shifted an average of 43$^{\circ}$ to a more
easterly pattern in 2000.  Observational measurements from
this time period corroborate an unusual wind and resulting
ice cover pattern in winter 2000-2001 (Clement et al.
2004).  The dramatic response in sea ice and ocean
conditions to this weather pattern suggests that wind is
the dominant forcing mechanism in the northern Bering Sea.
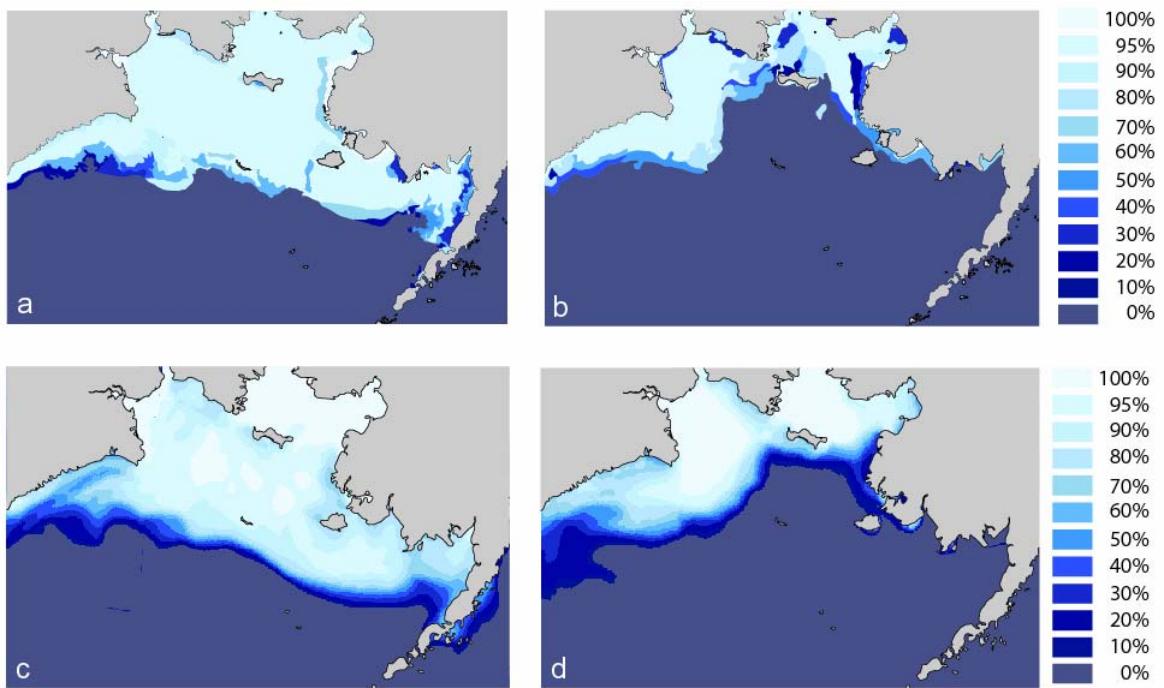
Figure 19.        Sea ice concentration on (a) February 19,
        1999 and (b) February 19, 2001 as determined using
          data obtained from the U.S. National Ice Center
        (From Clement et al., 2004).  Model monthly mean sea
        ice concentration during (c) February 1999 and (d)
                        February 2001.
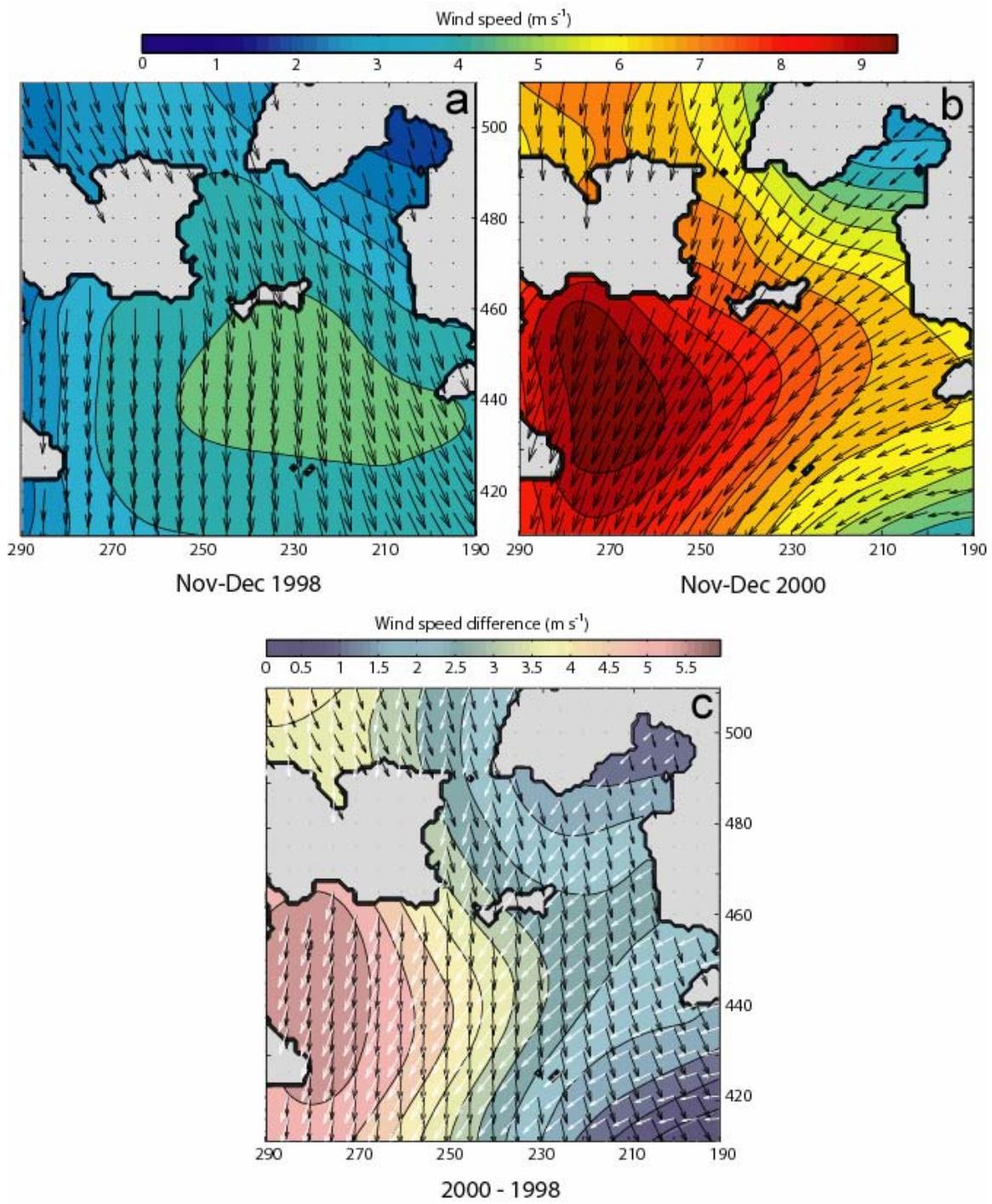
Figure 20.        Model wind forcing fields averaged over
        November and December (a) 1998 and (b) 2000. (c) The
        magnitude difference (2000-1998) and both wind
        fields (1998 in black; 2000 in white).

The correlation of the Bering Strait volume transport (13-month running mean of monthly means for 1979-2001) with several time series of large-scale weather indices has also been examined. The correlation with the Arctic Oscillation (AO) is negative with a correlation coefficient (r = -0.51) with the AO leading Bering Strait transport by 3 months. Therefore, the AO can explain approximately 26% ($r^2$ * 100) of the variance in the Bering Strait transport. Bering Strait transport is positively correlated (r = 0.53) with the Pacific Decadal Oscillation (PDO) explaining ~28% of the variance, while the Pacific-North America Index (PNA) has a correlation coefficient of 0.39, explaining ~15% of the transport variance. The time lag that gives the highest correlation with the PDO and PNA is approximately three years. The PDO and PNA are not independent, as they incorporate similar weather information. Assuming the PDO/PNA and AO are independent, the combined effect of the AO and the PDO/PNA can explain ~41-54% of the total variance of the Bering Strait transport. The complexity of the air-sea interactions between atmospheric forcing and the Bering Sea circulation prevent us from precisely pinpointing the mechanisms underlying these correlations. The remaining transport variance (~46-59%) is likely due to a combination of synoptic and/or local weather patterns, sea ice conditions, and ocean circulation.

Average heat transport (2.37 TW, S.D. = ±4.12 TW) across Bering Strait, indicates a net flux of warm water (relative to the reference temperature of -0.1$^{\mathrm{o}}$C) to the north (Fig. 21). There were summer peaks upwards of 20 TW when warm water transited northward (1979, 1990, 1994, and 1999). The annual average heat transport ranged from 1.29

47

(during 1983) to 4.28 TW (during 1979) over a semi-cyclic time period of 3-5 years. Unlike freshwater transport, heat transport across all the sections does not appear to be directly linked to volume transport, but instead has a unique pattern of variability controlled by changes in both water temperature and flow direction.
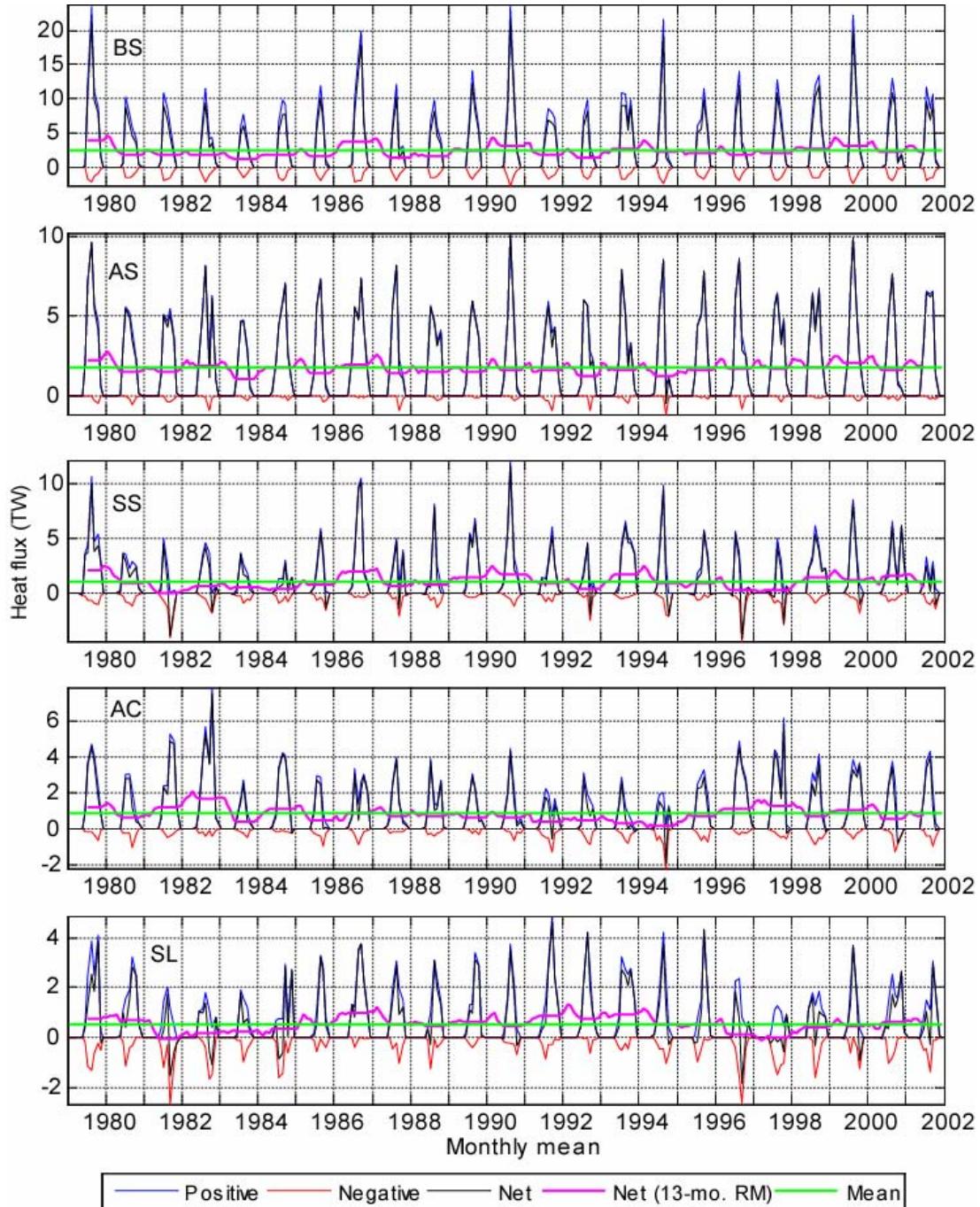
Figure 21.        Monthly mean heat fluxes over a 23-year time
series.  Positive (blue line) fluxes represent flow
to the North or East according to the model grid
(see Figure 8), while negative (red line) fluxes
represent flow to the South or West.  Black lines
represent net flow.  The smoothed net flux (thick
magenta line) is a 13-month running mean.  The 23-yr
mean is represented by the green line.  The
reference temperature is -0.1($^{o}$C).

The low-salinity, nutrient-rich water flowing northward through Bering Strait is important for maintaining the stratification, as well as constraining nutrient budgets, of the Arctic Ocean (Cooper et al., 1997 and references therein). Based on data collected during the 1970's and 1980's (e.g. Coachman and Aagaard, 1988; Aagaard and Carmack, 1989) the Bering Strait freshwater inflow into the Arctic Ocean is estimated to be ~1670 $km^3$ $yr^{-1}$, referenced against 34.8 psu. Modeled freshwater transport across Bering Strait for 1979-2001 averaged 46,842 $m^3$ $s^{-1}$ when normalized against salinity of 34.8. This translates into 1477 $km^3$ $yr^{-1}$ (standard deviation of ±192 $km^3$ $yr^{-1}$, or ~13%) over the 23-year simulation. Interannual variability in freshwater transport is high with values ranging from 981 (during 1994) to 1955 $km^3$ $yr^{-1}$ (during 1979). Freshwater transport (Fig. 22) is highly correlated with volume transport at Bering Strait (r = 0.93). High correlations also exist for AS (r = 0.95) and SS (r = 0.97). Anadyr Strait contributes approximately 78% of the freshwater flux through Bering Strait, while Shpanberg Strait contributes the remaining 22%. These percentage contributions are comparable to the respective percentage contributions of volume transport mentioned earlier.
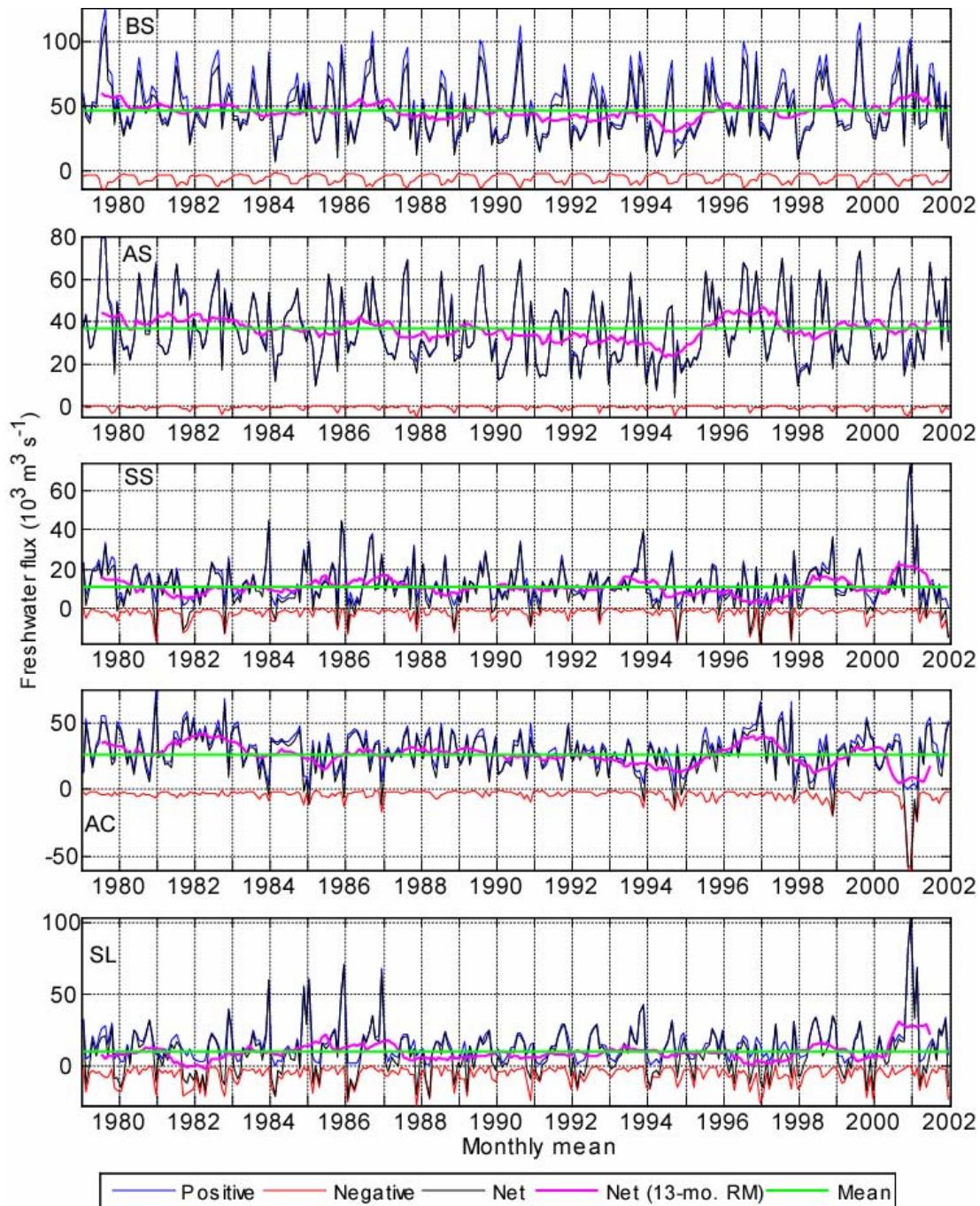
Figure 22.        Monthly mean freshwater fluxes over a 23-
year time series.  Positive (blue line) fluxes
represent flow to the North or East according to the
model grid (see Figure 8), while negative (red line)
fluxes represent flow to the South or West.  Black
lines represent net flow.  The smoothed net flux
(thick magenta line) is a 13-month running mean.
The 23-yr mean is represented by the green line.
The reference salinity is 34.8.

## 4.  Three-Dimensional Circulation and Water Column Structure

Flow over the northern Bering Sea is complex in both the horizontal and vertical dimensions (Fig. 23).  This is especially true in Bering Strait, where the highest northward velocities (up to 0.45 m s$^{-1}$ in the 23-yr mean) occur in the deep channels of the strait, while slower or southward flows occur in the center and closer to the coasts of the 85-km-wide strait.  The reversal of the flow in the center may be due to a stylized representation of the Diomede Islands at this model resolution.  A local intensification of the flow is modeled near the western coast, with the 23-year mean velocities greater than 0.10 m s$^{-1}$, which represents the northward extension of the Anadyr Current upstream.  Velocities in Bering Strait are most highly correlated with the upstream velocities in Anadyr Strait ($r = 0.83$) and, to a lesser degree, with those in Shpanberg Strait ($r = 0.64$).  These values are similar to those obtained by Coachman (1993) based on data from current meter moorings in Bering, Anadyr, and Shpanberg straits.  In Anadyr Strait there are two velocity cores (>0.06 m s$^{-1}$) over the flanks of the strait, with stronger flow (>0.10 m s$^{-1}$) along the Siberian side at depth 10-35 m (Fig. 23). Similarly, Shpanberg Strait shows a separation of flow with a higher velocity (>0.05 m s$^{-1}$) near St. Lawrence Island.  The Anadyr Current, which flows through Anadyr Strait, with a velocity core of over 0.12 m s$^{-1}$ in the 23-year mean is represented as a narrow (~70-km-wide) coastal current.  The St. Lawrence section shows a

southeastward flow up to 0.06 m s$^{-1}$ near the island with a sluggish northwestward flow further offshore.
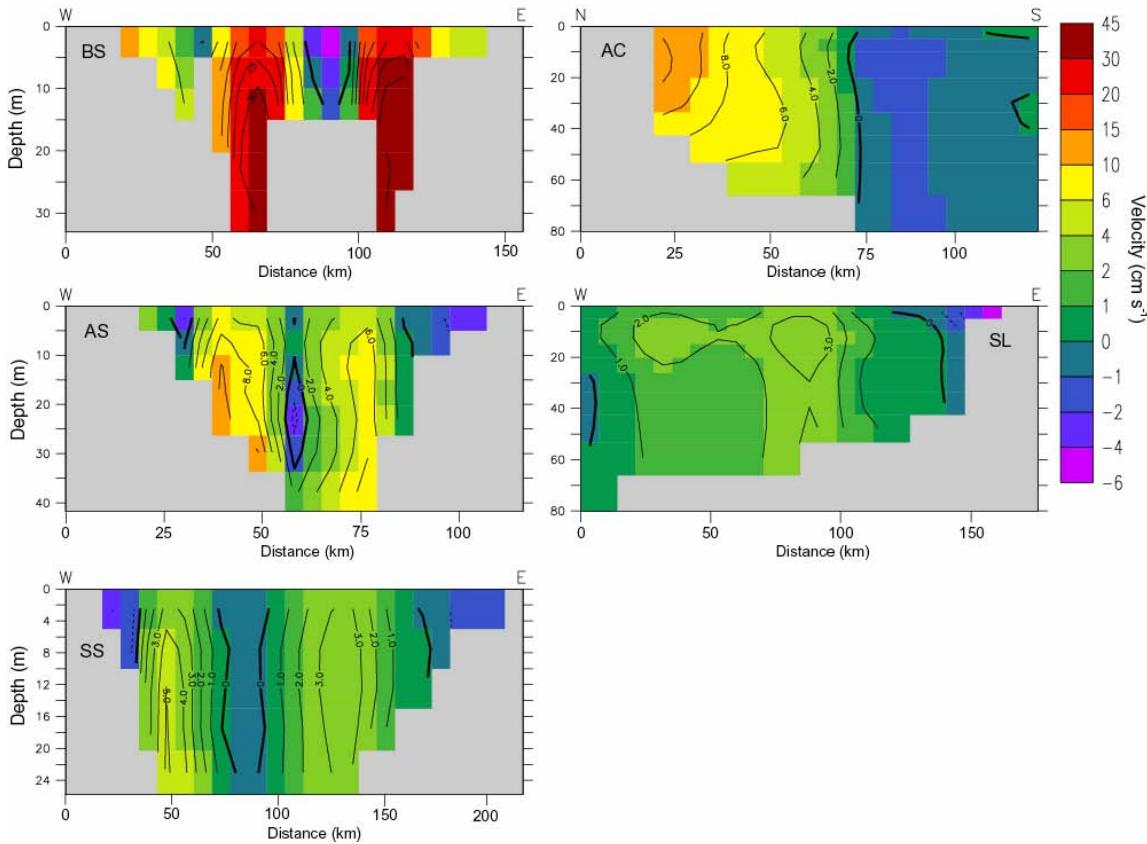


Figure 23.      Twenty-three-year mean (1979-2001) profiles of velocity (cm s$^{-1}$) for various sections.  Positive velocity is directed northward or eastward (AC).


As discussed earlier, velocities in Bering Strait are seasonally variable with lower values occurring during winter under sea ice cover (data not shown).  The Bering Strait velocity cores are located in the deep western and eastern channels with wintertime monthly mean speeds of 0.2 - 0.4 m s$^{-1}$.  During summer, after the sea ice is removed, core velocities increases to 0.4 - 0.6 m s$^{-1}$, and the cores vertically extend from near-bottom into shallow depths, sometimes up to the surface (July and August).  Throughout

the year velocities in the eastern channel tend to exceed velocities in the western channel (by ~0.05 – 0.15 m s$^{-1}$). Such differences in velocity and water mass properties (as discussed below) are especially important when interpreting data only from the U.S. (eastern) side of the strait.

Mean temperatures for the sections range from -1.8 $^{o}$C near-bottom in the St. Lawrence section to 4 $^{o}$C at the surface in the eastern part of Shpanberg Strait (Fig. 26). The east-west gradient across Bering Strait is clearly reflected in the colder water from Anadyr Strait to the west and the warmer water from Shpanberg Strait to the east. However, the 23-year mean surface water temperatures in both Anadyr and Shpanberg Straits is warmer than Bering Strait surface water temperatures.
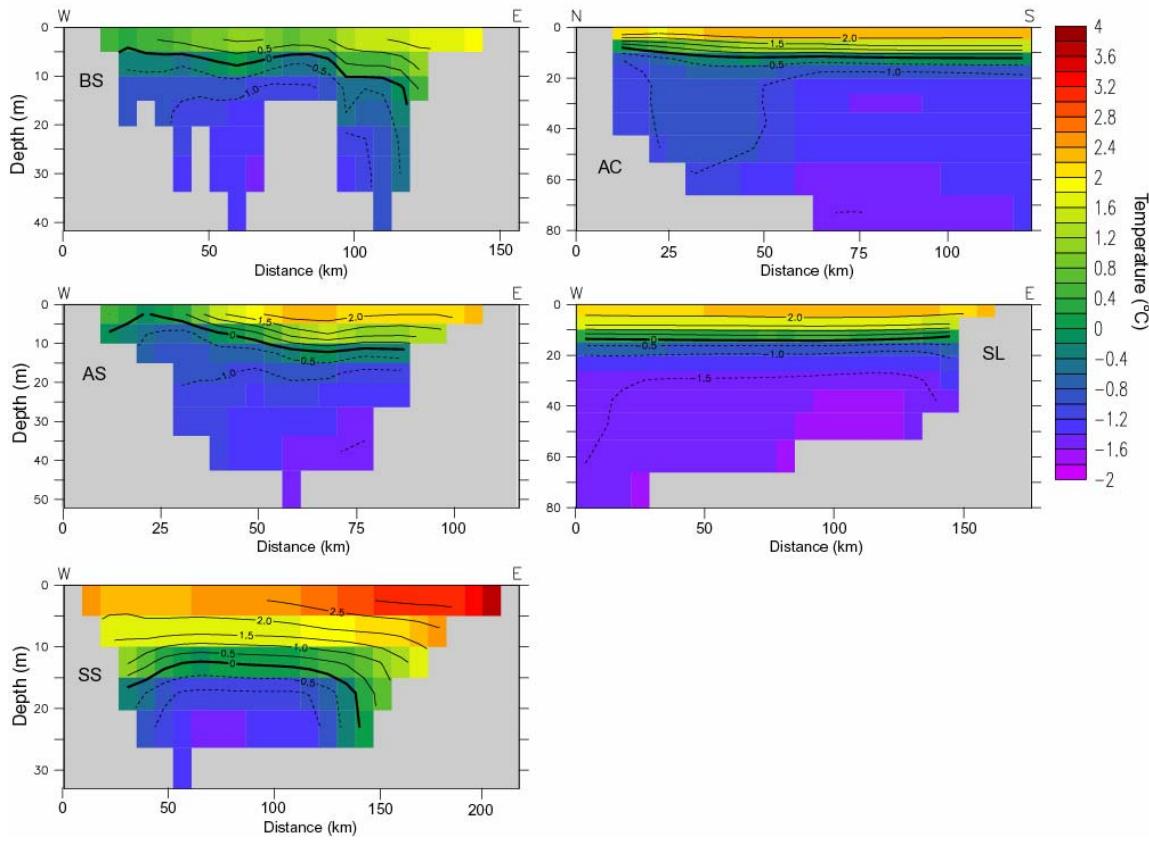
Figure 24.        Twenty-three-year mean (1979-2001) profiles
                of temperature ($^{\circ}$C) for various sections.

Salinity ranges from 31.4 to 33.2 across Bering
Strait, with fresher water at the surface and on the
eastern side of the section due to the contribution of
Alaska Coastal Water entering through Shpanberg Strait
(Fig. 25).   The salinity maximum in the core of Anadyr
Current is advected, after a slight dilution, through
Anadyr Strait into to the deep, western channel of Bering
Strait.   The high and low salinity signals are moderated as
water flows northward toward Bering Strait, which suggests
mixing north of St. Lawrence Island.   However, an east-west
gradient across Bering Strait remains, due to the dominant
contributions from upstream water masses.
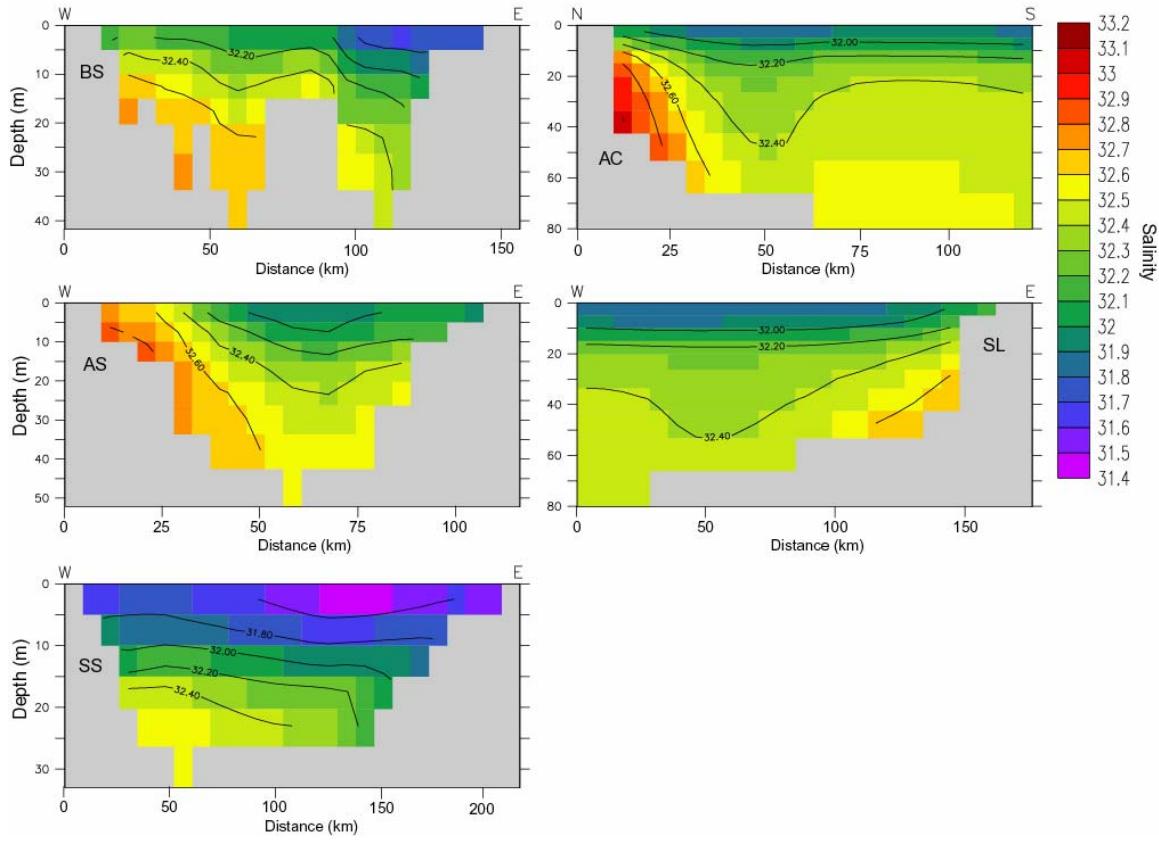
Figure 25.        Twenty-three-year mean (1979-2001) profiles
                of salinity for various sections.

Twenty-three year mean seasonal changes in the northern Bering Sea were analyzed at 4 vertical stations: in the deepest part of Anadyr, Shpanberg, and Bering (western and eastern channels) straits (respectively light blue, green, blue and red lines in Figs. 26-28; see Figure 8 for station locations). Temperatures for all stations were isothermal near the freezing point of seawater from December through April (Fig. 26). Surface warming developed first in AS and SS during May and the water temperature reached $10.5^{\circ}C$ at the surface by July. Warming in the western and eastern channels of Bering Strait

56

followed AS and SS warming, reaching 8 and 10$^{\circ}$C, respectively, by August.  It is interesting to note that from July to October surface waters in AS and SS were warmer than the downstream Bering Strait, while deeper water remained significantly cooler in the upstream locations.  This warming of deeper Bering Strait water (especially in the eastern channel) may be a result of warm water coming from Norton Sound and subsequent mixing between St. Lawrence Island and Bering Strait.  The bottom of the thermocline was at ~10 m in July and deepened to 15-20 m in September.
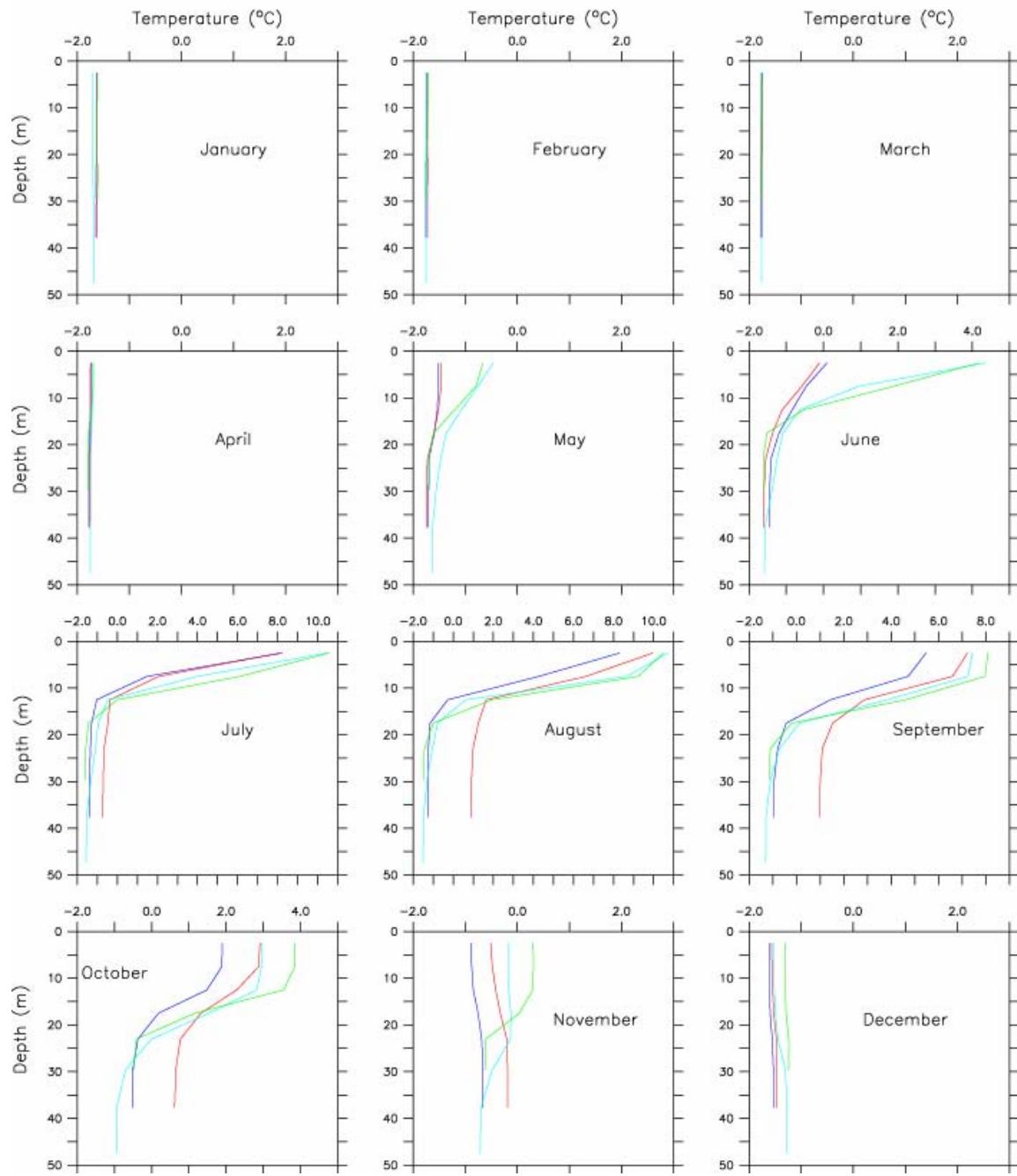
Figure 26.        Monthly mean vertical profiles of temperature (°C) at various model stations taken at the deepest point in each channel or strait (see Fig. 8). The stations are the East (red) and West (blue) channels of Bering Strait, Anadyr Strait (light blue), and Shpanberg Strait (green).

During winter, the stations show very little vertical salinity structure (Fig. 27), however as ice melt begins during spring, SS begins to develop a low salinity surface layer in April with other sections following in May and June.  The eastern channel of Bering Strait has the lowest surface salinity (S = 30) in July, as peak river discharges from the Yukon and other Alaskan rivers are entrained within the northward flowing Alaska Coastal Current.  The density profiles (Fig. 28) are very similar to the salinity profiles, which is not surprising at low temperatures.  The monthly mean density (over 23-years) across the Bering Strait section shows a persistent east-west gradient over the entire year with higher density to the west (not shown).   Stronger stratification sets in during June, primarily due to sea ice melt and runoff, and lasts through September and October.
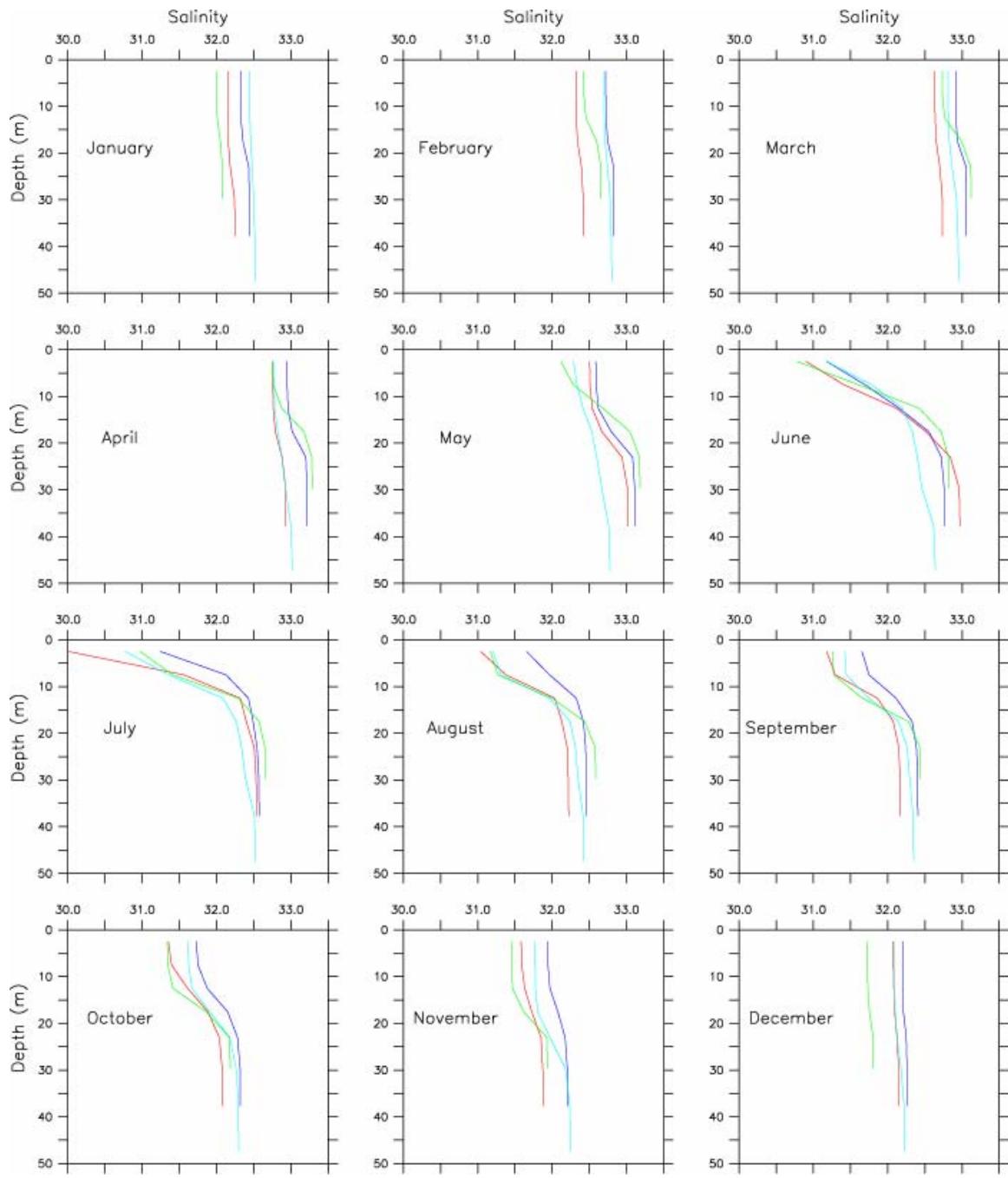
Figure 27.        Monthly mean vertical profiles of salinity
       at various model stations taken at the deepest point
       in each channel or strait (see Fig. 8). The stations
            are the East (red) and West (blue) channels of
                Bering Strait, Anadyr Strait (light blue), and
                          Shpanberg Strait (green).

60
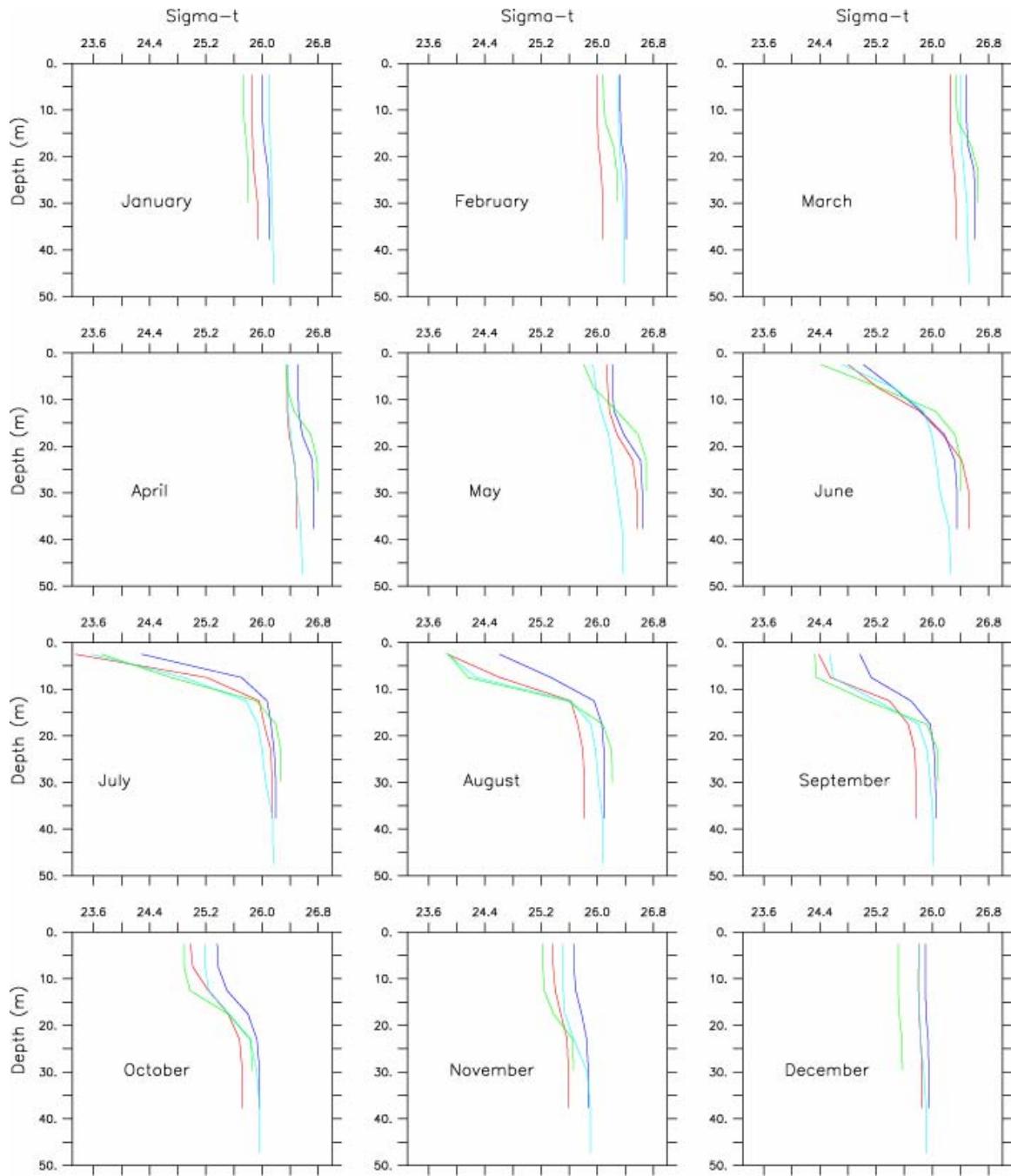
Figure 28.     Monthly mean vertical profiles of sigma-t at
various model stations taken at the deepest point in
each channel or strait (see Fig. ?). The stations
are the East (red) and West (blue) channels of
Bering Strait, Anadyr Strait (light blue), and
Shpanberg Strait (green).

As mentioned earlier, vertical sections of temperature (Fig. 26) indicate the possibility of vertical mixing, leading to warming of deeper water after it passes through AS and SS. Alternatively, or perhaps in addition, the cooling in the upper water column north of St. Lawrence Island in the Chirikov Basin could be involved. To examine the possibility of these processes, a T-S plot is provided for the three main sections (AS, SS, and BS; Fig. 29). This shows that waters at BS are similar to AS with slightly lower density near the surface because of the SS influence. For depth levels 12.5 m and 17.5 m, BS is actually denser than AS suggesting the possibility of cooling and/or sea ice formation north of St. Lawrence Island.
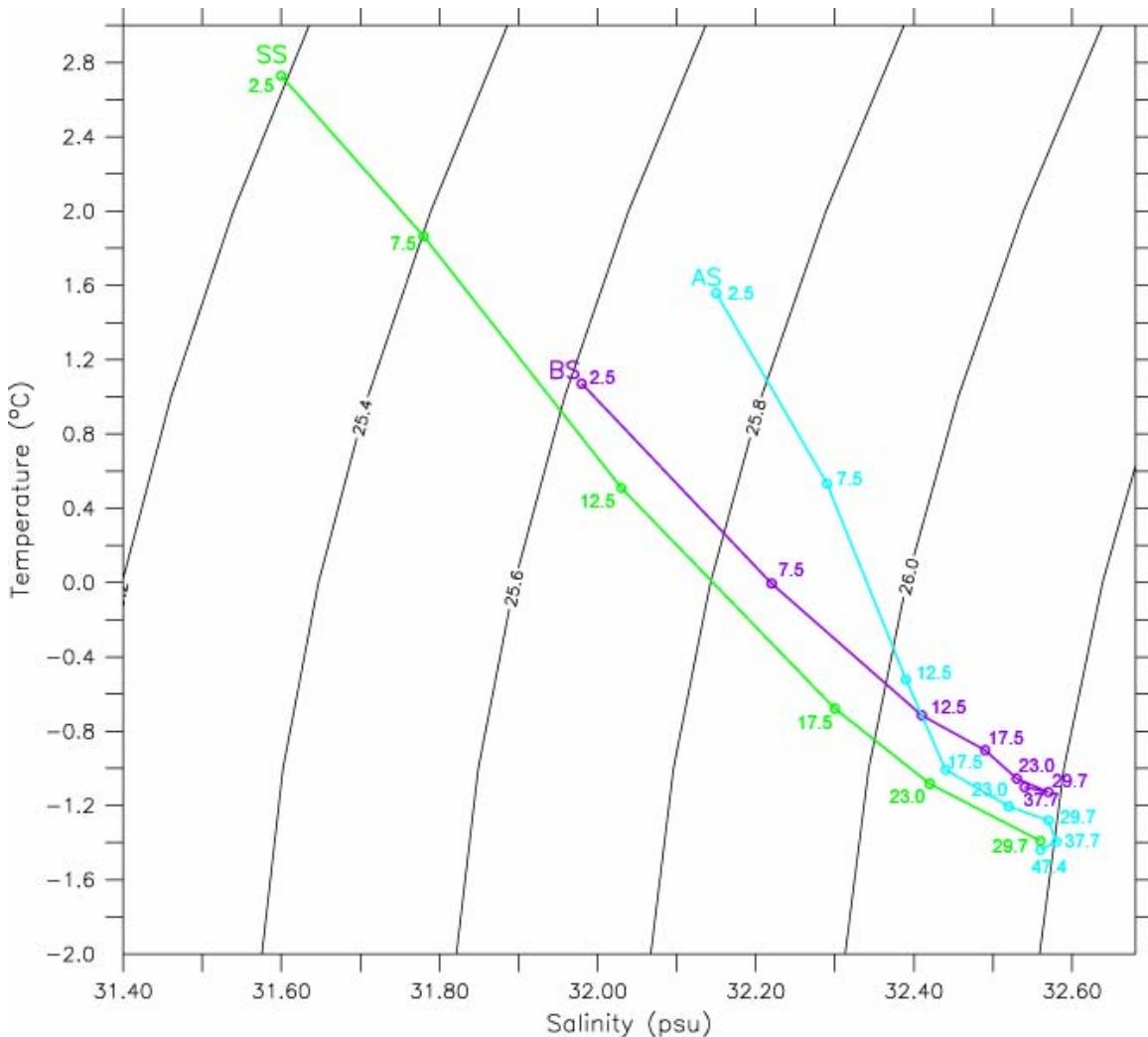
Figure 29.        Twenty-three-year mean (1979-2001) T-S
        diagram.  Numbers represent the depth of each
      section.  T-S values are a horizontal mean across
     each section.  Bering Strait (purple), Anadyr Strait
          (light blue), and Shpanberg Strait (green).


## 5.    Model-Data Validation at Bering Strait


Three moorings in the vicinity of Bering Strait have
produced time series of velocity, salinity, and temperature
(Roach et al., 1995; Woodgate et al., 2005).    Mooring
locations were in the western channel, eastern channel, and

just north of Bering Strait with instruments placed approximately 10 m above the bottom (locations shown in Fig. 8). There has been only limited access to the western channel location through international collaboration, because it lies in Russian territorial waters. First, salinity and temperature data for 1990-2001 (courtesy of K. Aagaard, R. Woodgate, and T. Weingartner website: http://psc.apl.washington.edu/HLD/Bstrait/bstrait.html) are compared with model output (Fig. 30). There is a clear seasonal cycle in salinity and temperature from both the observational and model time series. Results show that the model salinities are within the range of the observations, but there is somewhat less variability in the model output. The observational data show a salinity range of approximately 1.5 psu over each annual cycle, while the model range is only about 1.2 psu. Model salinities also tend to be higher than observations. A significant peak in salinity during 1991 is reflected in both the modeled and observational time series. Over the annual cycle, temperatures have a range of approximately 2 to 6.5$^{\circ}$C in the model output, while in the observational dataset the range is 4 – 8$^{\circ}$C. In both the model output and the observational data the eastern channel is almost always warmer than the western channel and northern location. Summer temperatures in the western channel and to the north are generally lower in the model than in observations. In the eastern channel, the modeled temperature agrees quite well with the data, however there are some years when the model shows colder temperatures in summer. It is possible that the depth at which the observations were made and the model depth may be inconsistent and could lead to different values of salinity and temperature shown in Fig. 30. In addition,

observations are at a single depth compared to model values representing a layer with thickness ranging from 5 to 10 m in the upper 50 m.
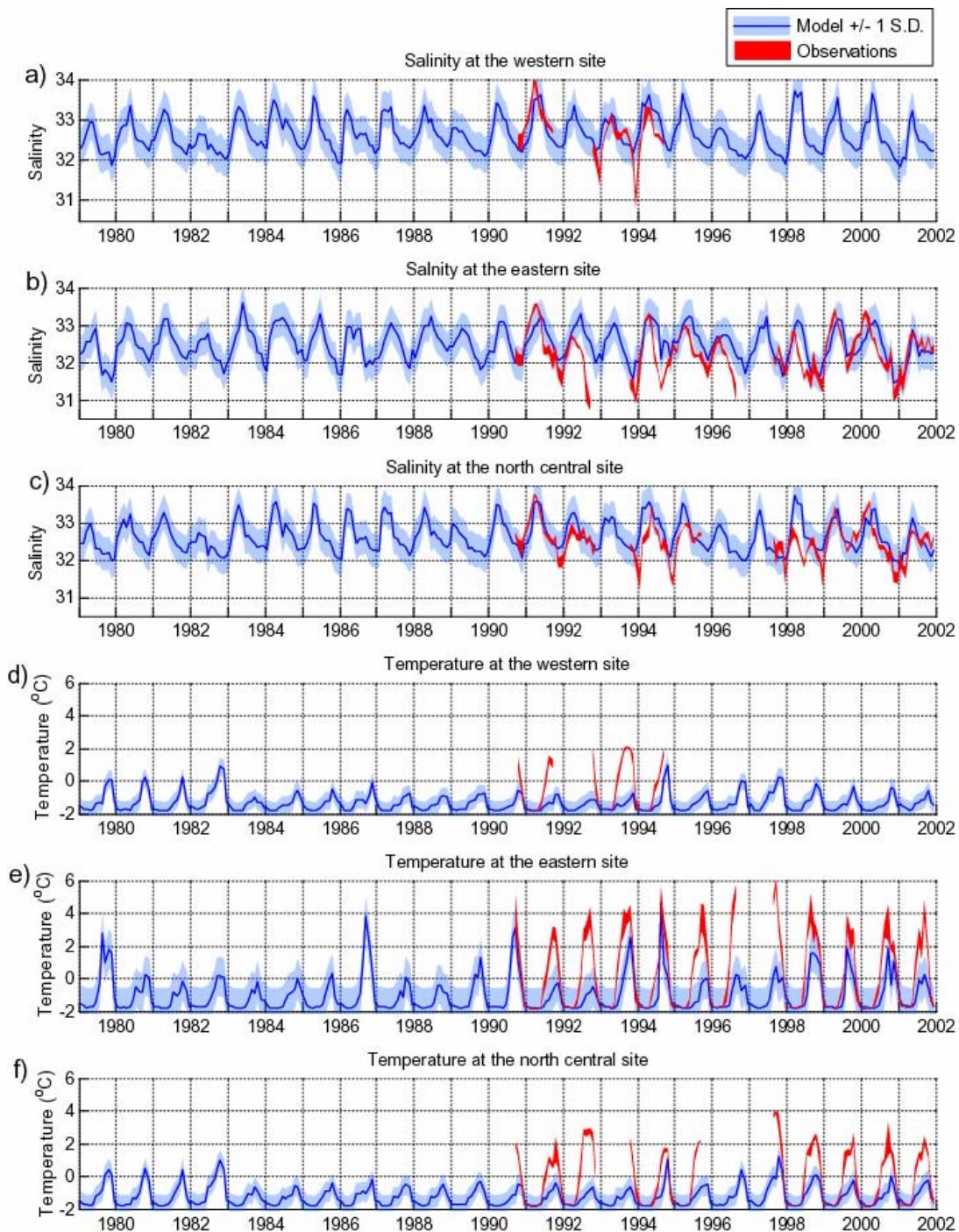
Figure 30.      Bering Strait monthly mean salinity (a,b,c)
        and temperature (d,e,f) as measured at three
      moorings at ~10 m above the bottom (red) and from
      the model (blue).   Observations include associated
      error and modeled values are shown with shading
      representative of +/- 1 S.D.  (Observations are
        courtesy of K. Aagaard, R. Woodgate, and T.
                       Weingartner.
                          66

An important time scale to consider in the Bering Strait volume transport is the annual cycle. The available estimates adapted from Coachman & Aagaard [1988; herein after referred to as C & A (1988)] and Roach et al. (1995), along with model estimates calculated via two different methods are shown in Figure 31. The first method (green line in Fig. 31) is an integral of velocity multiplied by sectional area at each model grid point along the Bering Strait section. The second method (dashed blue line in Fig. 31) represents the product of velocity at a single point near the bottom of the Eastern Channel (i.e. the location of eastern mooring from Roach et al. 1995) and a constant cross-sectional area (2.6 $km^2$). The second calculation allows direct comparison with observational estimates based on the same method (Woodgate et al., 2005) using velocity from the single deep mooring in the eastern channel. The methods of Roach et al. (1995) are less straightforward, however, results suggest they are similar to those of Woodgate et al. (2005) except they combine intermittent velocities from three near-bottom moorings in and north of Bering Strait during October 1990 – October 1994 and use regression techniques to fill in the data gaps. The C & A (1988) estimate is based on various short-term (less than one year) measurements and correlation with the wind field from 1946 – 1985. The Roach et al. (1995) study also extends C & A (1988) estimations from geostrophic wind through 1992. All four estimates are similar in that they show higher transport in summer and lower values in winter (Fig. 31). The modeled transports are most similar to the C & A (1988) estimates and are typically within one standard deviation of these observations. Exceptions are

during May, when the second method is slightly higher and
during June and July, when the first method is slightly
lower.    The Roach et al. (1995) estimate has a more
pronounced annual cycle and is in excess of one standard
deviation above the C & A (1988) estimate during May-July.
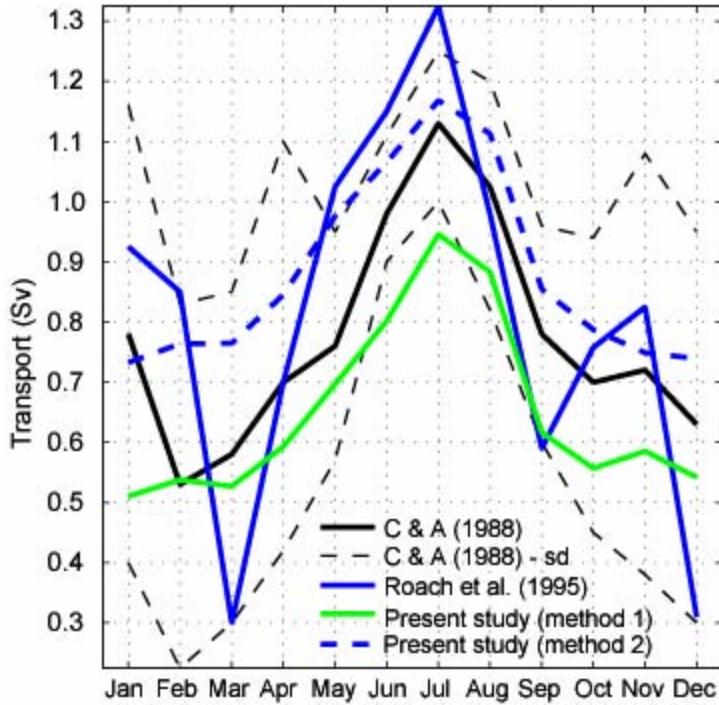


Figure 31.      Bering Strait annual cycle transport
    (monthly means) from various studies.  The Coachman
    and Aagaard (1988) estimate is shown in black with
    standard deviation lines in dashed black.  The Roach
    et al. (1995) estimate is shown in solid blue.  The
       model estimates were made via two methods.  The
     first method (in green) utilizes the entire strait
     in both the horizontal and vertical directions and
      is the method used for other calculations in this
     paper.  The second method (in dashed blue) is done
        by using only the near-bottom velocity in the
     eastern channel multiplied by a cross-sectional area
                       (2.6 km$^2$).

Expanding the comparison of the two methods for calculating the modeled transport, it is observed that an estimate derived as a product of velocity at a single point and a constant cross-sectional area (method 2; as in Woodgate et al., 2005) yields an average transport of 0.80 Sv for the period October 1990-October 1994 (Fig. 32). This value is close to the observational estimate of 0.83 Sv reported by Roach et al. (1995; Fig. 11). The other model method (method 1), which utilizes velocity information for the entire strait, yields a lower transport of 0.582 Sv or ~73% of the first method estimate. In conclusion, observational estimates utilizing only one point measurement of near-bottom velocity in the eastern channel of Bering Strait may overestimate the volume transport through the strait by up to 27%.
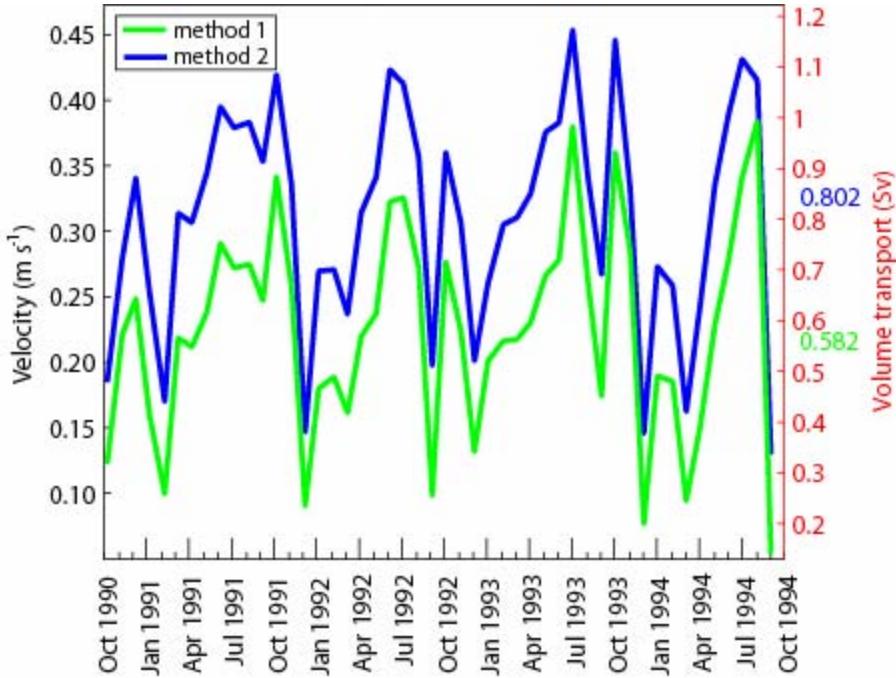
Figure 32.        Bering Strait monthly mean transport during
          October 1990 – October 1994 estimated from the model
            using two methods.  The first method (in green)
             utilizes the entire strait in both the horizontal
          and vertical directions and is the method used for
          other calculations in this paper.  The second method
            (in dashed blue) is done by using only the near-
          bottom velocity in the eastern channel multiplied by
          a cross-sectional area (2.6 km$^2$).  Means for the
             time series are shown on the right axis in the
                          respective colors.


     Bering Strait transport varies also at the interannual
time  scale.    As  in  Figure  31,  Figure  33  shows  three
observational  estimates  of  annual  mean  values  adapted  from
previous   studies   along   with   the   model   results.     In
addition,  we  also  show  some  recent  estimates  based  on
velocities   in   the   Eastern   Channel   and   north   central
moorings  (and   the   constant   cross-sectional   area,   as
previously  mentioned).  These  estimates  are  courtesy  of  R.
Woodgate  and  are  based  on  data  presented  in  a  recent  paper
70

(Woodgate, et al. 2005). The modeled transport (green line, method 1) on average represents 88% of the observational estimates during 1979-1994, ranging from 34% in 1994 to 115% in 1980. (For this calculation, observational estimates were averaged when more than one estimate occurred.) The simpler model method (dashed blue line, method 2) on average represents 117% of the observational estimates during 1979-1994, ranging from 60% in 1994 to 157% in 1980. The model estimates for 1990-1994 using this method are in a similar range as the observational estimates (0.68 – 1.14 Sv), however, particular annual means do not necessarily overlap. It is important to note here that the Roach et al. (1995) estimate for 1994 did not include October – December, which typically have lower monthly mean transport values. This may partially account for the relatively high transport value reported for 1994. Similarly, the 1990 mean estimate is based on October - December data only, which explains its lower value. Additional uncertainty with comparison of model and Roach et al. (1995) estimates has to do with regression methods used to determine vertical velocity shear and transport during gaps in direct measurements in the deep channels of the strait. When examining the annual mean transport values, it appears that the model (method 1) is most similar to observations from 1979-1988 and, in fact, during that time the model estimates average 98% of observational estimates (ranging from 84% in 1982 to 115% in 1980). The recent estimates made by Woodgate et al. (2005) tend to fall between the two methods of calculation from the model output. Annual mean volume transport based on data from the Eastern Channel (magenta circles) can be higher or lower than transport based on data from the north

central mooring (blue circles).  Associated errors in all observational and model datasets make distinguishing between years difficult.
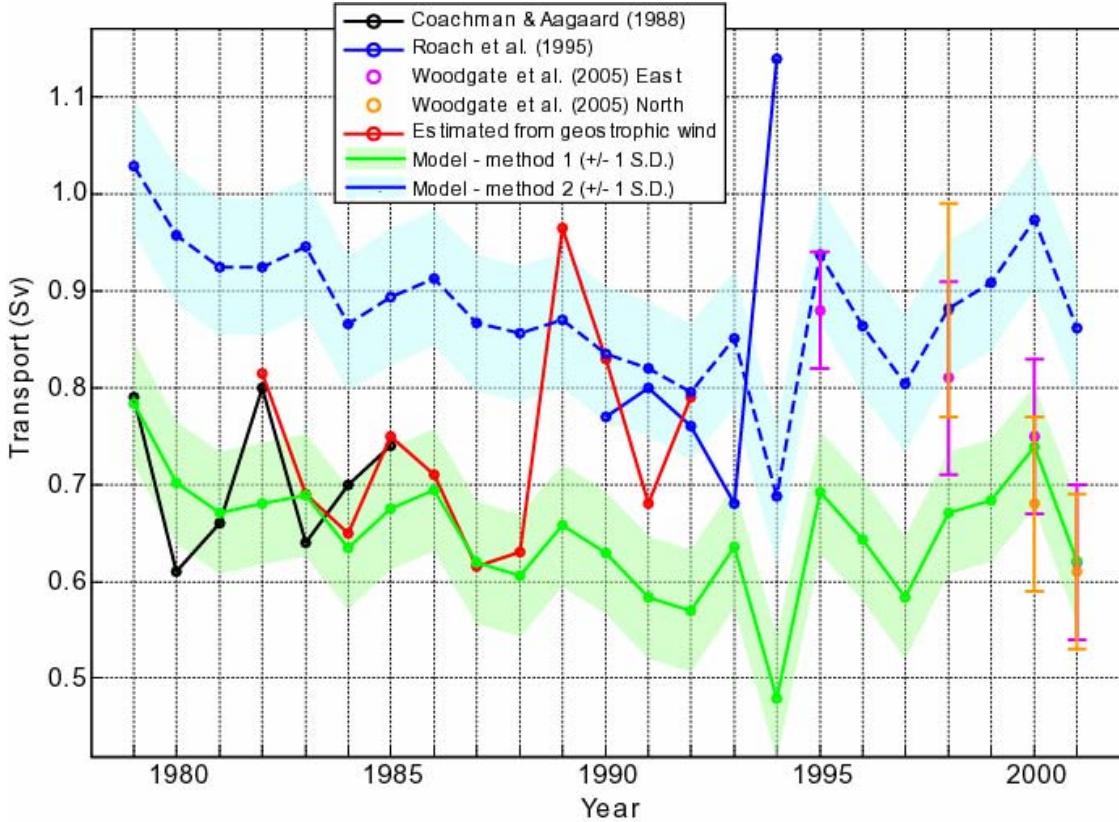


Figure 33.        Bering Strait annual mean transport from various studies during 1979 – 2001.  The Coachman and Aagaard (1988) estimate is shown in black and the Roach et al. (1995) estimate is shown in solid blue.  The estimation from geostrophic wind (red line) was given in Roach et al. (1995).  Estimates from Woodgate et al. (2005) are shown as magenta (Eastern Channel mooring) and orange circles (north central mooring).  These estimates include error bars.  The model estimates were made via two methods.  The first method (in green) utilizes the entire strait in both the horizontal and vertical directions and is the method used for other calculations in this paper.  The second method (in dashed blue) is done by using only the near-bottom velocity in the eastern channel multiplied by a cross-sectional area (2.6 km$^2$).  For the model estimates, the green and blue shading represent +/- 1 S. D.

## 6. Comparison with Observations of Salinity and Nutrients

Comparisons of the modeled salinity field were made against field observations from eight cruises during the period 1988 – 1999 from April through September (Figs. 34 and 35). In this analysis the salinity at the deepest field sample depth is compared to the salinity at the lowest model level. In the observational dataset, the deepest sample depth is approximately 5 - 10 m above the seabed and the deepest level in the model represents a layer from 5 - 70 m thick in the upper 400 m where almost all observations occur. Note that salinity is correlated with nutrient concentrations in the Bering Sea in the deeper parts of the water column and/or below the euphotic zone (present study statistics and discussion to follow; Phyllis Stabeno, pers. comm.). Therefore, a significant correlation between the model and observed salinities may give insight into the deeper water column nutrient concentrations in the Bering Sea.
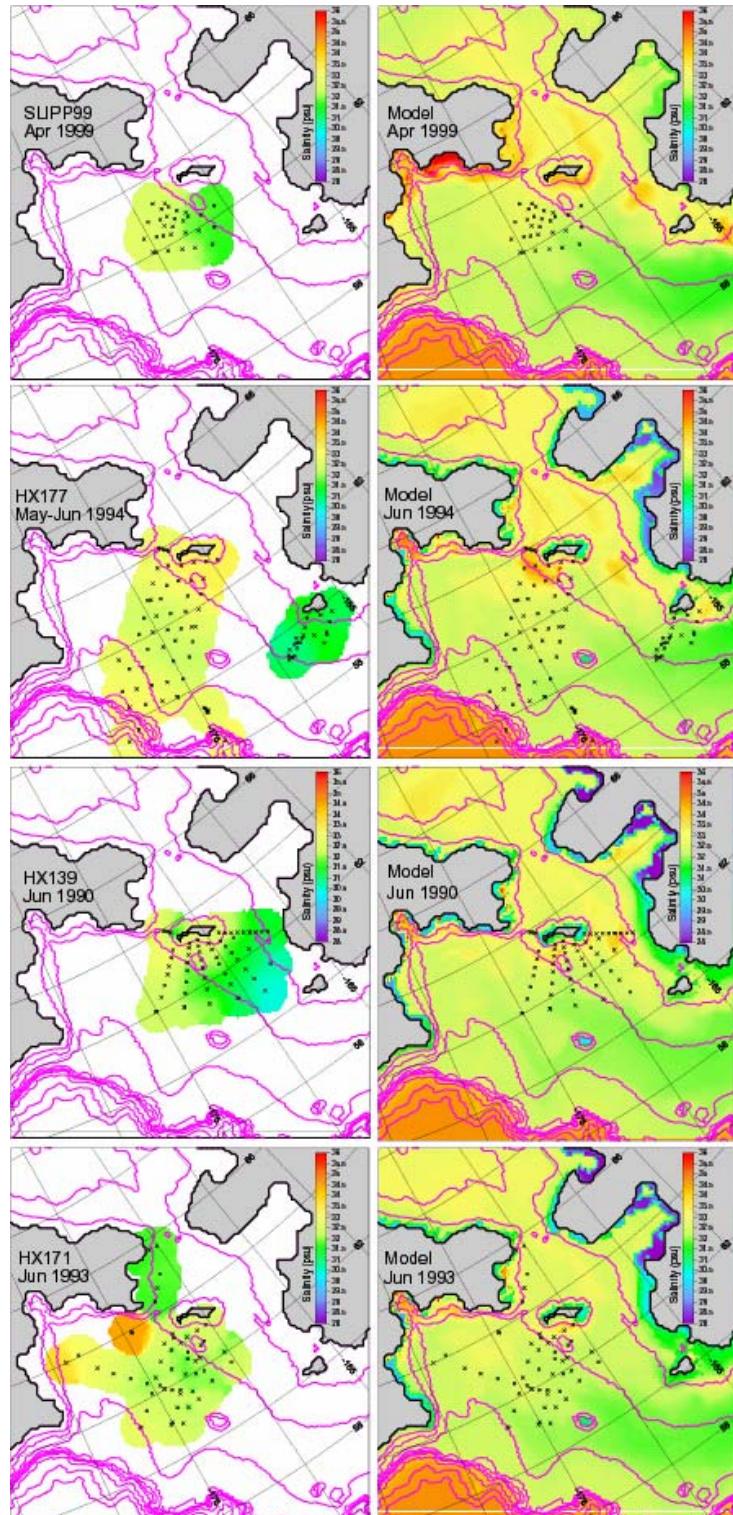
Figure 34.     Comparison of near bottom salinity between
        cruise observations (left) and model output (right)
            during late winter through early summer.
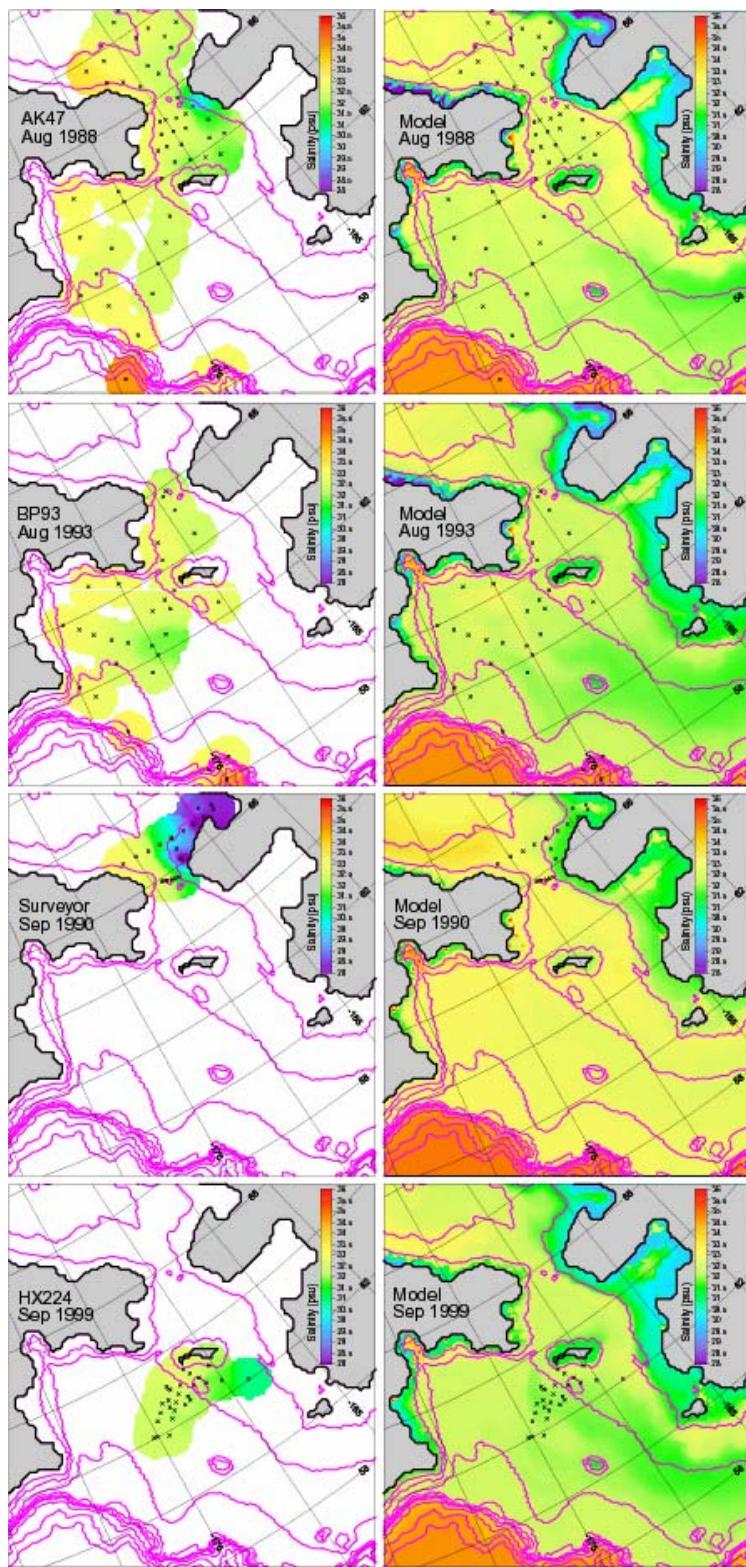
Figure 35.     Comparison of near bottom salinity between
cruise observations (left) and model output (right)
during summer through early autumn.

A significant (significance level, $\alpha$ = 0.01) correlation occurs between observed and modeled salinity in all of the eight cruises combined (sample size = 346; correlation coefficient, r = 0.47, p-value < 0.01). The p-value is a measure of how much evidence is against the null hypothesis (i.e. a small p-value means the correlation is significant). Correlation coefficients for individual cruises range from -0.32 in June 1990 to 0.96 during September 1990. The mean salinity difference for all cruises combined is 0.246, with the model having higher salinity than observations. For individual cruises, the salinity difference ranges from -0.226 in August 1993 when the model is less saline than observations to 0.949 in September 1990 when the model is more saline than observations. It is important to note here that a strong correlation is not always associated with a small mean salinity difference and vice versa.

In general, the model agrees with observations showing fresher water in the east and more saline water in the west (Figs. 34 and 35), although there appears to be a deficit of the freshwater flux in the Alaska Coastal Current in the model. This and other relatively narrow coastal currents may not be fully resolved at the present model resolution (e.g. Maslowski and Walczowski, 2002). With respect to the freshwater input, the model directly incorporates runoff from the Yukon River, but not from the Kuskokwim, Naknek and other more southerly sources. In the model, relatively fresh water is found near the coast, but is likely constrained to a narrower path than in reality. For example, a horizontal freshwater intrusion extends along

76

the bottom from about 30-70 m depth from the southeast toward the northwest (Figs. 34 and 35). The extent and intensity of this tongue of freshwater exhibits seasonal and interannual variability. Model salinities are generally in a smaller range than the observations, therefore, east-west gradients are somewhat muted in the current version of the model. However, it is important to note that field observations for each cruise were collected instantaneously at individual stations over the course of approximately one month, while the model output is the mean salinity of one month. In addition, the field observations are sampled from water that is approximately 5 - 10 m above the bottom, which may or may not be the same depth as the deepest model grid level. In addition, the bottom boundary layer physics occur in the model in a vertical layer, which in most cases is thicker than the real boundary layer.

Finally, a potential relationship between observed nutrients (i.e. silicate) and salinity is analyzed to show potential utility of using model salinity and EKE information as a proxy for nutrient distribution in deep shelf waters. The shelf of the northern Bering Sea is supplied by upwelling of high-silica water from the deep basin (Tsunogai et al., 1979). Near-bottom field observations of silicate concentrations (Fig. 36) and salinity (Figs. 34 and 35) over the Bering shelf have a similar distribution. In fact, a significant correlation exists between the two parameters (sample size = 340; $r$ = 0.56; $p < 0.01$) when data from all cruises are combined. The correlation coefficients for individual cruises range between 0.60 and 0.78, except in September 1990 when the correlation coefficient was 0.43. This is possibly due to

the extremely low salinity that was present in and around the Kotzebue Sound, likely due to a strong mixing of the river runoff signal.
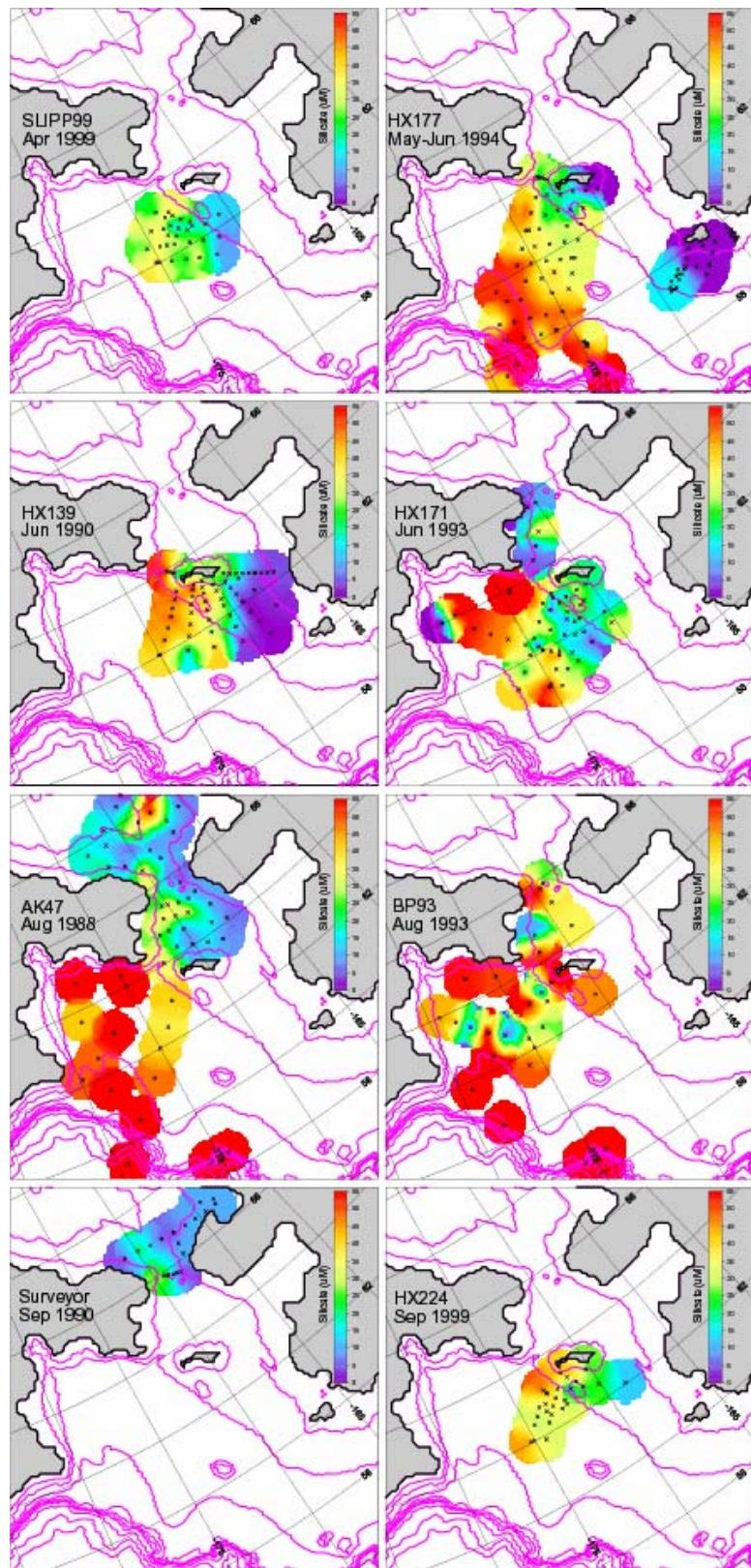
Figure 36.          Silicate concentration (μM) in near bottom
            samples collected during various cruises.

In general, the analyzed silicate concentration has an apparent east-west increase across the Bering shelf. As already mentioned, western and/or deeper stations have higher silicate concentrations due to the upwelling of nutrient-rich deep Bering Sea Water. High silicate concentrations are measured in the Gulf of Anadyr and become diluted and biologically utilized downstream, as this water moves northward toward Bering Strait. The significant correlation between observed salinity and silicate concentration supports the idea that salinity can be a proxy for silicate concentration in near-bottom waters of the Bering Sea. Therefore, regions of high salinity, which are just downstream from regions characterized by highly energetic mixing, may support higher primary production through vertical movement of nutrients into the euphotic zone. Specifically, these regions of known high primary and secondary (benthic) productivity, or 'hot spots', include the Chirikov Basin and the region just north of Bering Strait (Grebmeier et al. 1988; Springer and McRoy, 1993; and Grebmeier and Dunton, 2000). The high modeled EKE (Figs. 6, 7, 12, 13) combined with high salinity derived from the nutrient-rich Anadyr Water (Fig. 34 and 35) allows for higher biological production in these areas. It can be inferred that improved model simulations of the distribution of ocean salinity and eddies (EKE) could provide useful information about biological 'hot spots' and other high productivity regions.

# IV. DISCUSSION

Volume transport through Bering Strait is estimated to be 0.65 Sv over the 23-year simulation, while Roach et al. (1995) estimate approximately 0.83 Sv during October 1990–October 1994. When model output is compared for the same time interval, the model estimate is 0.58 Sv. The differences in these transport volumes may arise due to several factors. A possible source of discrepancy between observations and model results is the model atmospheric forcing fields, which are smoothed and of relatively low resolution, making the model less likely to simulate strong, local events. However, the observational estimates are based on point measurements and regressions to short time-series of ADCP velocity measurements, while the model calculations integrate over horizontal and vertical axes and are numerically continuous in time. Both methods have associated errors, but the model results suggest that estimates of the Bering Strait transport derived from one point measurement are higher (~27%) than the estimates derived from a method which utilizes velocities across the entire strait. According to the long-term mean model output (Fig. 23), near-bottom velocities in the eastern and western channels of the Bering Strait are the highest of any point across the strait. This provides a very reasonable explanation of why observational estimates based on velocity time series at one or two points generally give higher transport values.

The modeled freshwater flux through Bering Strait indicates a wide range of interannual variation (981 – 1955 km$^3$ yr$^{-1}$) and this variation is strongly linked to the

overall volume transport. Because the model tends to have higher salinity than observations, this flux may be in some instances an underestimate of the actual freshwater flux. Modulation and variation of the northward freshwater flux has implications for Chukchi Sea and Arctic Ocean stratification and nutrient budgets.

The northward heat transport is also interannually variable (1.29 – 4.28 TW), however, it is largely independent of volume transport. It is also worth pointing out limitations to the field observations when used for similar flux calculations. The observations are made intermittently at three mooring locations in the Bering Strait region and then are extrapolated to represent the entire section, which according to the model results experiences significant, seasonally dependent, horizontal and vertical gradients of water properties and flow structure.

In quantifying the circulation and water mass properties of the northern Bering Sea, time scales from a few days to interannual and decadal have been considered. Model estimates of the annual cycle of Bering Strait transport are most similar to those based on geostrophic winds and wind forcing has been shown to be an important factor in Bering Sea circulation. Although the annual cycle is particularly important because of the high seasonality of flow through Bering Strait and the seasonally variable energy levels (EKE) across the shelf, model results indicate that short-term events, such as the flow reversal in winter 2000-01, and interannual variability also have a strong impact on the regional circulation and property distribution.

In order to determine the characteristics of water flowing through Bering Strait, it is important to consider upstream conditions. In the model it is observed that water from Anadyr Strait contributes 80% of the mean flow (23-year mean = 0.52 Sv) into the Chukchi Sea. The wider, but shallower Shpanberg Strait contributes only 20% (0.13 Sv) of the mean flow through Bering Strait. It is worth noting that not all of the water flowing through Anadyr Strait is associated with the Anadyr Current. Instead, some water moving northward on the northern Bering shelf can also go west around St. Lawrence Island through Anadyr Strait to reach Bering Strait.

Since the majority of Bering Strait throughflow is associated with the Anadyr Current, it is important to observe the characteristics of this water. However, most of Anadyr Strait lies in Russian territorial waters and international research efforts have been significantly limited in this area. Additional scientific efforts and field observations including long-term moorings in the Gulf of Anadyr and on the western side of Bering Strait, would be critical for determining the characteristics of the Pacific inflow into the Chirikov Basin north of St. Lawrence Island and eventually into the Arctic Ocean through the Bering Strait. Such data would allow further validation and constraining of ocean models for climate study.

Modeled temperature shows an east-west gradient across the northern Bering shelf, similar to observations (e.g. Coachman, 1987; Grebmeier et al. 1988), due to the presence of relatively warm Alaska Coastal Water to the east and cold Anadyr Water to the west. A smaller north-south

gradient exists in the 23-year mean surface water temperature, with slightly lower temperatures in Bering Strait as compared to Anadyr Strait. This cooling north of St. Lawrence Island (SLI) may be due to several factors, such as the presence of winter polynyas and ice production north of SLI and in Norton Sound (Pease, 1980) and flow reversals in Bering Strait, especially during autumn.

Comparisons of modeled and observed salinities show that the model represents both the general east-west gradient and the seasonal changes associated with sea ice formation and melt. Future model improvements will include more realistic representation of the salinity and temperature impacts from additional freshwater sources in the region. The ability to explicitly resolve the warm, fresh Alaska Coastal Current would enhance salinity representation from the Gulf of Alaska into the Bering Sea and further downstream in the Arctic Ocean. Modeled vertical sections across the two Pacific Water pathways toward Bering Strait show narrow coastal currents (< 30 km) and separation of flow. With the present model resolution (~9 km) such scales are not fully resolved. Higher resolution will also be critical for resolving eddies, which have been demonstrated to be important for the circulation in the northern Bering Sea (Figs. 6, 7, 12, 13). Also, tides are known to be important in many areas for ocean mixing and overall circulation. However, tides across the northern Bering shelf are much weaker compared to those over the southeast shelf and Aleutian Island regions (Kowalik, 1999) so their absence may not be highly detrimental to the overall model results.

Because silicate concentrations can be estimated to some degree by salinity in sub-euphotic waters in the Bering Sea, this model has the potential to provide insights into the nutrient distribution across the shelf and through Bering Strait. This is especially important in regions that have been understudied, such as the Gulf of Anadyr and the western side of Bering Strait. Coincidentally, these same locations are thought to have high salinities and nutrient concentrations, which are important for biological production in the water column and the benthos. In addition, such information might be useful for the initialization and forcing of biological models using output from the physical model.

THIS PAGE INTENTIONALLY LEFT BLANK

# V.  CONCLUSIONS

Mean velocity and total kinetic energy fields from the model generally show northward transport across the Bering Sea shelf with high velocity in narrow straits, such as Bering and Anadyr straits.  The analyses suggest that the observational estimates of transport through Bering Strait might be overestimated by as much as 27%.  The importance of flow through Anadyr Strait is emphasized in its dominant contribution to Bering Strait throughflow and the similar seasonal and interannual patterns of water properties and flow observed in both Anadyr and Bering straits.  Long-term measurements in that region would be critical for model validation and improvement.  Time series of volume transport show that the model is able to represent anomalous events, such as major flow reversals, which are corroborated by observations.  Wind appears to be the dominant force driving water and ice movement across the northern Bering Sea at synoptic to interannual time scales. In addition to wind forcing, it is also important to consider buoyancy forcing along the Alaska coast, which is enhanced by runoff from Alaskan rivers.  Comparisons of modeled salinities with salinity observations show that the model is able to reproduce the characteristics of major water masses across the Bering shelf and in Bering Strait. However, incorporation of additional river sources and higher model resolution is needed, especially to improve representation of the lower salinity ranges in the Alaska Coastal Current along the southwestern Alaskan coast.  EKE fields show that the NBS maintains year-round high energy and mixing, especially in Bering and Anadyr straits.

Notably, these regions of high EKE are found just upstream of highly productive areas in the Bering Sea (e.g. the Chirikov Basin and the region just north of Bering Strait) that have been identified in previous studies such as Grebmeier et al. (1988), Springer and McRoy (1993), and Grebmeier and Dunton (2000).   This suggests that high-nutrient Anadyr Water is mixed into the euphotic zone as it flows generally northward and, upon encountering a region of lower EKE, can support water column primary production and the settling of organic matter to the benthos.

# LIST OF REFERENCES

Aagaard, K., and E. C. Carmack, The role of sea ice and other fresh water in the Arctic circulation, *J. Geophys. Res., 94*, 14485-14498, 1989.

Aagaard, K., A. T. Roach, and J. D. Schumacher, On the wind-driven variability of the flow through Bering Strait, *J. Geophys. Res., 90*, 7213-7221, 1985.

Cavalieri, D. J., P. Gloersen, C. L. Parkinson, J. C. Comiso, H. J. Zwally, Observed hemispheric asymmetry in global sea ice changes, *Science, 278*, 1104-1106, 1997.

Clement, J. L., L. W. Cooper, and J. M. Grebmeier, Late winter water column and sea ice conditions in the northern Bering Sea, *J. Geophys. Res., 109(C3)*, C03022, doi:10.1029/2003JC002047, 2004.

Coachman, L. K., Advection and mixing on the Bering-Chukchi Shelves. Component A. Advection and mixing of coastal water on high latitude shelves, ISHTAR 1986 Progress Report, Vol. I. Inst. Mar. Sci., Univ. Alaska, Fairbanks, p. 1-42, 1987.

Coachman, L. K., On the flow field in the Chirikov Basin, *Cont. Shelf Res., 13*, 481-508, 1993.

Coachman, L. K., and K. Aagaard, Transports through Bering Strait: annual and interannual variability, *J. Geophys. Res., 93*, 15535-15539, 1988.

Cooper, L. W., T. E. Whitledge, J. M. Grebmeier, and T. Weingartner, The nutrient, salinity, and stable oxygen isotope composition of Bering and Chukchi seas waters in and near the Bering Strait, *J. Geophys. Res., 102*, 12563-12573, 1997.

Goosse H., J. M. Campin, T. Fichefet, and E. Deleersnijder, Sensitivity of a global ice-ocean model to the Bering Strait throughflow, *Clim. Dynam., 13(5)*, 349-358, 1997.

Grebmeier, J. M., and L. W. Cooper, Influence of the St. Lawrence Island Polynya upon the Bering Sea benthos, *J. Geophys. Res. 100*, 4439-4460, 1995.

Grebmeier, J. M., and K. H. Dunton, Benthic processes in the northern Bering/Chukchi seas: Status and global change, in *Impacts of changes in sea ice and other environmental parameters in the Arctic*, edited by H. P. Huntington, pp. 61-71, Report of the Marine Mammal Commission Workshop, 15-17 February 2000, Girdwood, Alaska, 2000.

Grebmeier, J. M., C. P. McRoy, and H. M. Feder, Pelagic-benthic coupling on the shelf of the northern Bering and Chukchi seas. I. Food supply source and benthic biomass, *Mar. Ecol. Prog. Ser., 48*, 57-67, 1988.

Hermann, A. J., P. J. Stabeno, D. B. Haidvogel, and D. L. Musgrave, A regional tidal/subtidal circulation model of the southeastern Bering Sea: development, sensitivity analyses and hindcasting, *Deep-Sea Res. II, 49*, 5945-5967, 2002.

Jakobsson, M., N. Cherkis, J. Woodward, R. Macnab, and B. Coakley, New grid of Arctic bathymetry aids scientists and mapmakers, *Eos Trans. AGU, 81(9)*, 89, 2000.

Johannessen, O. M., E. V. Shalina, M. W. Miles, Satellite evidence for an Arctic sea ice cover in transformation, *Science, 286*, 1937-1939, 1999.

Kowalik, Z., Bering Sea Tides, in *The Bering Sea: Physical, Chemical and Biological Dynamics*, edited by T. R. Loughlin and K. O. Ohtani, pp. 93–127, Alaska Sea Grant Press, Fairbanks, AK, 1999.

Maslowski, W., D. Marble, W. Walczowski, U. Schauer, J. L. Clement, and A. J. Semtner, On climatological mass, heat, and salt transports through the Barents Sea and Fram Strait from a pan-Arctic coupled ice-ocean model simulation, *J. Geophys. Res., 109*, C03032, doi:10.1029/2001JC001039, 2004.

Maslowski, W., and W. Walczowski, Circulation of the Baltic Sea and its connection to the Pan-Arctic region – a large scale and high-resolution modeling approach, *Boreal Environ. Res., 7(4)*, 319-325, 2002.

Muench, R. D., and K. Ahlnäs, Ice movement and distribution in the Bering Sea from March to June 1974, *J. Geophys. Res., 81*, 4467-4476, 1976.

Nihoul, J. C. J., P. Adam, P. Brasseur, E. Deleersnijder, S. Djenidi, and J. Haus, Three-dimensional general circulation model of the northern Bering Sea's summer ecohydrodynamics, *Cont. Shelf Res., 13*, 509-542, 1993.

Overland, J. E., Marine climatology of the Bering Sea, in *The eastern Bering Sea shelf: Oceanography and resources, Vol. 1.*, edited by D. W. Hood and J. A. Calder, p. 15-22, University of Washington Press, Seattle, 1981.

Overland, J. E., and C. H. Pease, Cyclone climatology of the Bering Sea and its relation to sea ice extent, *Mon. Weather Rev., 110*, 5-13, 1982.

Overland, J. E., and A. T. Roach, Northward flow in the Bering and Chukchi seas, *J. Geophys. Res., 92*, 7097-7105, 1987.

Overland, J. E., M. C. Spillane, H. E. Hurlburt, and A. J. Wallcraft, A numerical study of the circulation of the Bering Sea basin and exchange with the North Pacific Ocean, *J. Phys. Oceanogr., 24*, 736-758, 1994.

Pease, C. H., Eastern Bering Sea ice process, *Mon. Weather Rev., 108*, 2015-2023, 1980.

Reed, R. K., On geostrophic reference levels in the Bering Sea Basin, *J. of Oceanogr., 51*, 489-498, 1995.

Roach, A. T., K. Aagaard, C. H. Pease, S. A. Salo, T. Weingartner, V. Pavlov, and M. Kulakov, Direct measurements of transport and water properties through the Bering Strait, *J. Geophys. Res., 100*, 18443-18457, 1995.

Royer, T. C., Baroclinic transport in the Gulf of Alaska, Part II. A fresh water driven coastal current, *J. Mar. Res. 39*, 251-266 , 1981.

Schumacher, J. D., K. Aagaard, C. H. Pease, R. B. Tripp, Effects of a shelf polynya on flow and water properties in the northern Bering Sea, *J. Geophys. Res., 88*, 2723-2732, 1983.

Spaulding, M., T. Isaji, D. Mendelsohn, A. C. Turner, Numerical simulation of wind-driven flow through the Bering Strait, *J. Phys. Oceano. 17*, 1799-1816, 1987.

Springer, A. M., and C. P. McRoy, The paradox of pelagic food webs in the northern Bering Sea. III. Patterns of primary production, *Cont. Shelf Res. 13*, 575-599, 1993.

Stabeno, P. J., N. A. Bond, N. K. Kachel, S. A. Salo, and J. D. Schumacher, On the temporal variability of the physical environment over the southeastern Bering Sea, *Fish. Oceano. 10(1)*, 81-98, 2001.

Stabeno, P. J., D. G. Kachel, N. B. Kachel, and M. E. Sullivan, Observations from moorings in the Aleutian Passes: temperature, salinity and transport, *Fish. Oceano., in press*, 2005.

Stabeno, P.J. and R. K. Reed, Circulation in the Bering Sea basin by satellite tracked drifters, *J. Phys. Oceanogr., 24,* 848-854, 1994.


Steele, M., R. Morley, and W. Ermold, PHC: A global ocean hydrography with a high quality Arctic Ocean, *J. Clim., 14(9)*, 2079-2087, 2000.


Tsunogai, S., M. Kusakabe, H. Iizumi, I. Koike, and A. Hattori, Hydrographic features of the deep water of the Bering Sea – the sea of silica, *Deep-Sea Res. 26A*, 641-659, 1979.


Walsh, J. J., C. P. McRoy, L. K. Coachman, J. J. Goering, J. J. Nihoul, T. E. Whitledge, T. H.Blackburn, P. L. Parker, C. D. Wirick, P. G. Shuert, J. M. Grebmeier, A. M. Springer, R. D. Tripp, D. A. Hansell, S. Djenidi, E. Deleersnijder, K. Henriksen, B. A. Lund, P. Andersen, F. E. Müller-Karger, and K. Dean, Carbon and nitrogen cycling within the Bering/Chukchi seas: source regions for organic matter effecting AOU demands of the Arctic Ocean, *Prog. Oceano., 22*, 277-359, 1989.


Woodgate, R. A., K. Aagaard, and T. Weingartner, Monthly temperature, salinity, and transport variability in the Bering Strait throughflow. *Geophys. Res. Lett.*, 32(4), doi: 10.1029/2004GL021880, 2005.

THIS PAGE INTENTIONALLY LEFT BLANK

# INITIAL DISTRIBUTION LIST

1. Defense Technical Information Center
    Ft. Belvoir, Virginia

2. Dudley Knox Library
    Naval Postgraduate School
    Monterey, California

3. Dr. Wieslaw Maslowski
    Department of Oceanography
    Naval Postgraduate School
    Monterey, California

4. Dr. Stephen Okkonen
    Institute of Marine Science
    University of Alaska
    Fairbanks, Alaska

5. Dr. Mary Batteen
    Department of Oceanography
    Naval Postgraduate School
    Monterey, California